

# Kinetics and retention of polystyrene sulfonate for proteoglycan replacement in cartilage

*Shalini Sundar*<sup>1</sup>, *Allison Koopman*<sup>2</sup>, *Thomas J. Manzoni*<sup>3</sup>, *Weiran Xie*<sup>2</sup>, *Qurat-Ul-Ain Bhatti*<sup>2</sup>,  
*Chun-Yuan Lo*<sup>4</sup>, *Vidhika S. Damani*<sup>2</sup>, *Ai Nin Yang*<sup>4</sup>, *Darrin Pochan*<sup>2</sup>, *Justin Parreno*<sup>1,3</sup>, *Julie B. Engiles*<sup>5,6</sup>, *Laure V. Kayser*<sup>2,4</sup>, *Charles Dhong*<sup>\*1,2</sup>

*\* Author to whom correspondence should be addressed: [cdhong@udel.edu](mailto:cdhong@udel.edu)*

1. Department of Biomedical Engineering, University of Delaware, Newark, DE, 19716, USA

2. Department of Materials Science and Engineering, University of Delaware, Newark, DE, 19716, USA

3. Department of Biological Sciences, University of Delaware, Newark, DE, 19716, USA

4. Department of Chemistry and Biochemistry, University of Delaware, Newark, DE, 19716, USA

5. Department of Clinical Studies, University of Pennsylvania School of Veterinary Medicine, Kennett Square, PA, 19348, USA

6. Department of Pathobiology, University of Pennsylvania School of Veterinary Medicine, Kennett Square, PA, 19348, USA

## 1. ABSTRACT

Tissue hydration provides articular cartilage with dynamic viscoelastic properties, crucial to its function. Early osteoarthritis (OA) is marked by loss of proteoglycans and glycosaminoglycans (GAG), lowering fixed charge density, and impairing tissue function. The most common GAG replacement, chondroitin sulfate, has failed to show effectiveness. Here, we investigated a synthetic polyelectrolyte, poly(styrene sulfonate) (PSS), both as a model compound to investigate polyelectrolyte transport in cartilage, and as a potential candidate to restore bulk fixed charge density in cartilage with GAG loss. Through bovine explants and histology, we determined zonal-based effective diffusion coefficients for three different molecular weights of PSS. Compared to chondroitin sulfate, PSS was retained longer in GAG-depleted cartilage in static and compression-based desorption experiments. We explained enhanced solute performance of PSS by its more compact morphology and higher charge density by SAXS. This may improve design of GAG mimetic molecules for repairing osmotic function in OA cartilage.

**KEYWORDS:** GAG replacement, proteoglycan replacement, osteoarthritis, fixed charge density, synthetic polyelectrolytes

## 2. INTRODUCTION

Despite the high prevalence of osteoarthritis (OA), there are no effective therapeutic strategies that significantly recover impaired cartilage osmotic function during disease progression.<sup>1</sup> While the collagenous matrix network provides cartilage with an intrinsic stiffness, interstitial fluid content within the tissue provides cartilage with crucial viscoelastic properties for repeated loading and lubrication.<sup>2,3</sup> Tissue hydration is driven by negatively charged glycosaminoglycan (GAG) side chains, which are linear-chained polysaccharides functionalized with sulfate groups

and covalently attached to proteoglycans that are embedded throughout the collagenous extracellular matrix.<sup>3</sup> Negative charges derived from GAGs give rise to a fixed charge density in cartilage and the subsequent Donnan ionic effect, which ultimately contributes 85% of the total osmotic pressure within the tissue.<sup>4,5</sup> During early stages of OA, matrix GAG content decreases considerably due to increased enzymatic degradation as well as age-related variations in synthesis.<sup>6,7</sup> This results in an initial loss of water retention and lubrication<sup>8-10</sup>, which ultimately makes the cartilage matrix more susceptible to further damage due to impaired load-bearing function.<sup>3,10</sup> Although several prior strategies have attempted to restore mechanical function in OA cartilage by stiffening the collagen network<sup>11,12</sup>, there has been comparatively fewer studies on restoring the osmotic function of tissue through proteoglycan replacements or GAG-based therapeutics.<sup>9,13</sup>

Traditional approaches have studied isolated GAGs, primarily chondroitin sulfate (CS), in combination with glucosamine, as an oral treatment for symptomatic OA<sup>14-16</sup>. However, results show conflicting clinical efficacy of using CS to treat OA<sup>17-19</sup>, in part due to the limited bioavailability (only 10% – 20%) from oral dosing<sup>14</sup>. CS as intra-articular injections has also been explored, however CS fails to effectively reduce the frictional coefficient of cartilage with GAG loss to native levels. Furthermore, CS is unable to effectively repair fluid load support in *ex vivo* cartilage explant studies.<sup>20,21</sup> Finally, due to inconsistent isolation and purification techniques, pharmaceutical and commercial grade CS often exhibit high structural heterogeneity and high contamination.<sup>22-24</sup> As CS is primarily obtained from animal sources such as bovine, porcine, avian or fish sources<sup>14,16</sup>, there is also a potential risk of transmittable zoonotic diseases<sup>25,26</sup>. These results question the effectiveness of using CS intra-articular injections as a prophylactic OA treatment and justifies the need for alternative GAG replacements.

Instead of using isolated CS, there has been a growing interest in developing alternative therapeutics that restore proteoglycan osmotic load-bearing function and tissue hydration in GAG-depleted cartilage.<sup>9,13</sup> While hydrogels functionalized with GAGs attempt to mimic some of the biochemical roles of GAGs within cartilage<sup>9,27</sup>, they do not directly replicate the biophysical and structural functions of GAG or proteoglycan molecules. These hydrogels are also susceptible to degradation *in vivo*, require *in vivo* crosslinking for utility and stability since CS is water soluble, and often require transplantation surgeries with complementary scaffold structures for mechanical integrity *in vivo*.<sup>27-29</sup> In an ideal format, injectable, non-degradable polyanionic hydrogels would be used to replace lost bulk fixed charge density, however, current options are limited.<sup>27,30</sup>

As an alternative to replacing the bulk-matrix through functionalized hydrogels, there has been interest in developing specialized mimetic molecules for intra-articular injections that restore or replace proteoglycan osmotic function.<sup>1,9</sup> For instance, Panitch and co-workers synthesize matrix binding peptides grafted to a CS backbone.<sup>31-33</sup> These molecules restored the bulk equilibrium compressive moduli in GAG-depleted cartilage explants<sup>33</sup>, but they are susceptible to digestion by native peptidases<sup>9</sup>, limiting their long-term retention and potential therapeutic benefit. In another approach, Marcolongo and co-workers grafted CS onto synthetic polymeric backbones, recreating the bottlebrush structure found in aggrecan without the susceptibility to enzymatic digestion found in recombinant proteoglycans.<sup>13,34-37</sup> While these compounds diffused quickly through the cartilage matrix, they primarily localized in the pericellular matrix, with a proposed mechanism of physical adhesive interactions with the native aggrecan network.<sup>35,37</sup> This specific localization may pose challenges during the delivery and adequate restoration of fixed charge density in cartilage with more significant aggrecan loss

during OA progression. Commercially available treatments primarily address the veterinary arthritis market and include brands like Adequan<sup>®</sup> (polysulfated GAGs) and Legend<sup>®</sup> (hyaluronate sodium).<sup>38</sup> While Adequan<sup>®</sup>, a heparin analogue, is primarily used for its anti-inflammatory benefits<sup>39</sup>, treatment has also been associated with clinical cases of hypocoagulation<sup>40,41</sup>. On the other hand, Legend<sup>®</sup> and other viscosupplementation treatments are primarily used to improve joint lubrication and may not directly restore bulk tissue osmotic function.

Overall, the development of GAG and proteoglycan analogues remains a critical area of research. An on-going challenge for designing such mimetic molecules has been elucidating the role of chemical structure and charge of polyelectrolytes on their solute transport properties within cartilage. Cartilage is an anisotropic, porous tissue with an effective pore size of approximately 6 nm<sup>42</sup>, and so the transport mechanics of therapeutic molecules are subject to factors arising from both the solute and tissue. For example, Travascio et al. showed that solute size has an inverse effect on diffusivity within the tissue (i.e., solutes with smaller Stokes radii had higher diffusion coefficients), and that diffusivity is also dependent on the tissue GAG content.<sup>43</sup> Furthermore, solutes with Stokes radii larger than the 6 nm effective pore size of cartilage were still able to rapidly diffuse through the tissue<sup>43</sup>, most probably because these molecules preferentially move between the collagen fibrils (which are spaced ~50 – 100 nm apart) instead of between the GAG molecules (which are spaced ~ 5 nm apart).<sup>44,45</sup> Broadly speaking, solutes can also display nonuniform diffusion kinetics that differ in each zone of cartilage. Leddy et al. found that moderate sized dextrans (40 kDa and 70 kDa) diffuse faster in the deep zone as compared to the superficial zone while smaller and larger sized dextrans (3 kDa

and 500 kDa) diffuse faster in the superficial zone as compared to the deep zone.<sup>46</sup> This indicates the presence of zonal size thresholds within cartilage.

Despite well-established studies on the transport of small molecules, the transport of larger polymeric structures is less understood. For instance, DiDomenico et al. demonstrated that the transport mechanics of linear and random-coil solutes, like polyelectrolytes, through cartilage is poorly predicted by traditional models based on spherical solutes<sup>45</sup>, and that flexible molecules can adjust their shape as they move through the anisotropic tissue, improving their diffusivity compared to similarly sized spherical molecules.<sup>44</sup> This indicates that solute shape has important consequences on the design of both semi-synthetic and synthetic GAG and proteoglycan mimics. Native aggrecan has a bottlebrush structure and native CS bristles are linear chained polysaccharides.<sup>47</sup> In addition to shape, charge plays a significant role on polyelectrolyte transport because of electrostatic interactions between the solute and the charged cartilage matrix. However, most research on polyelectrolyte transport and drug delivery has focused on polycationic molecules<sup>48–53</sup>, whereas aggrecan and CS are negatively charged polyanions. For example, Bajpayee and co-workers demonstrated that avidin, a positively charged molecule, displays higher partition coefficients than its neutrally charged counterpart, neutravidin.<sup>48,50</sup> Similar research on large polyanionic molecules remains limited.<sup>44,45</sup> Inarguably, solute size, charge and shape all affect delivery and retention of therapeutic molecules in cartilage, whose composition and structure undergo significant changes under traumatic loading and during OA disease progression. The design of GAG and proteoglycan replacements requires careful comprehension and optimization of the transport mechanics of these polyanionic compounds through the tissue.

Considering these challenges, we demonstrate how PSS can be used to synthetically replace lost bulk negative charge in cartilage with complete GAG loss and use it as a model polyelectrolyte to probe polyanion transport in cartilage. PSS is widely used as a reference polyelectrolyte standard in a variety of industries, since it is one of the few water-soluble polymers that has a high negative charge density with controllable molecular weight and dispersity.<sup>54</sup> PSS was also selected for its well-known solution dynamics (reasonably described by simple random coil dynamics<sup>54</sup>), for its immunity from cleavage by OA-associated enzymes due to its synthetic nature, and for its biocompatibility. PSS is currently used as a therapeutic to reduce total body potassium levels in patients with hyperkalemia<sup>55</sup>, and has also been used in drug discovery for its low cytotoxicity<sup>56-58</sup> and anti-microbial<sup>58</sup> properties. However, the application of PSS as a GAG substitute and its transport in hydrated soft tissue systems such as cartilage has not yet been experimentally explored.

We calculated the transport kinetics of PSS within bovine cartilage tissue that has been completely digested of GAG, as measured by Safranin-O staining. Effective zonal based diffusion coefficients of three different molecular weights of PSS (PSS-11kDa, PSS-20kDa and PSS-65kDa) were calculated, and the polymers were found to penetrate in faster from the deeper side than from the superficial side. Furthermore, while PSS treated cartilage demonstrated improved restoration and retention of negative charge, cartilage treated with chondroitin sulfate A (CS-A) displayed little to no such effectiveness. This enhanced delivery is hypothesized to be a result of the increased compact conformation of the PSS, which helps the polymer diffuse through and bind better with the tissue matrix. We also found molecular-weight dependent effects, and that of our three molecular weights, a considerable amount of PSS-65kDa was able to be retained for up to four days and upon loading at low compressive stresses. The results from this study address

the critical need and yields the design of proteoglycan and GAG analogues therapeutics that effectively restore tissue mechanical function in OA cartilage or improve the performance of synthetic biomaterials in whole-tissue replacements.

### 3. EXPERIMENTAL MATERIALS AND METHODS

**3.1. PSS Sample Preparation.** PSS synthesis was achieved using reversible addition-fragmentation chain-transfer (RAFT) polymerization. This method enables the facile synthesis of PSS with discrete molecular weights and low dispersity, but without the complexity or use of metals, as typically required in other controlled radical polymerization methods.<sup>59</sup> The following materials were used throughout: Sodium 4-styrenesulfonate (NaSS), 4,4'-azobis(4-cyanovaleric acid) (ACVA), the RAFT chain transfer agent (CTA) 4-cyano-4-(phenylcarbonothioylthio) pentanoic acid and hydrogen peroxide (H<sub>2</sub>O<sub>2</sub>) were all purchased from Sigma-Aldrich and used without further purification. Spectrum™ Spectra/Por™ 3 RC Dialysis Membrane Tubing 3500 Dalton MWCO was purchased through Fisher Scientific. Distilled water filtered using a Milli-Q purification system was also used throughout.

PSS was first synthesized following the procedure from Lo et al.<sup>60</sup>: NaSS (10 g, 48.50 mmol), 4-cyano-4-(phenylcarbonothioylthio) pentanoic acid (314.3 mg, 1.125 mmol) and ACVA (63.06 mg, 0.225 mmol) were added to a 100 mL single-neck, round-bottomed flask and dissolved in 33 mL water and 11 mL ethanol, before being degassed for 30 min under nitrogen. The reaction mixture was next placed into a 70 °C oil bath, and reacted for at least 16 h, after which it was stopped with rapid cooling and exposure to air. The PSS was purified by dialysis over a period of 16 h, before drying under heat and vacuum. The RAFT polymerization reaction scheme and reaction conditions have been provided in the Supporting Information (**Scheme S1**

**& Table S1).** Through this sample preparation procedure, we were able to achieve 100% fully sulfonated PSS that were subsequently used throughout the rest of this paper for tissue experimentation.

**3.2 Removal of RAFT agent.** The sulfur-based RAFT chain end group present in the PSS after the RAFT polymerization reaction may have unknown cytotoxicity issues, thus the dithiobenzoate end group was removed based on a procedure from Jesson et al.<sup>61</sup> Cleavage of the dithiobenzoate group occurred as follows: A 7.5% w/w solution of PSS (8.01 g, 0.0388 mol) in DI water (107 mL) was prepared and a 30% w/w aqueous solution of H<sub>2</sub>O<sub>2</sub> (0.42 mL, 0.00411 mol; H<sub>2</sub>O<sub>2</sub>:CTA molar ratio = 5:1) was added. The resulting solution was placed into a 70 °C oil bath and left open to air to react for 16 h. The solution was found to be acidic and was brought to pH = 7 using 5 M NaOH. The polymer was then dialyzed over a period of 16 h before drying under heat and vacuum to obtain the neat polymer. The cleavage reaction scheme and reaction conditions have been provided in the Supporting Information (**Scheme S2 & Table S2**). Confirmation of successful removal of the RAFT end group, indicated by the intrinsic color change of the samples, was determined using UV-Vis spectroscopy (**Figure S1 & Figure S2**).<sup>61</sup>

**3.3. Polymer Molecular Weight Characterization.** A gel permeation chromatography (GPC) system (HLC-8420 GPC EcoSEC LC, Tosoh) was run on 20% methanol and 80% 0.3 M NaNO<sub>3</sub>, 0.01 M NaH<sub>2</sub>PO<sub>4</sub> in water at 25 °C (0.8 mL min<sup>-1</sup>), using two PL Aquagel-OH Mixed-H (8 μm, 50 × 7.5) columns. The GPC system used was calibrated against narrow dispersity PSS standards (Polymer Standards Service) and was used to determine the number-average molar mass ( $M_n$ ), the weight-average molar mass ( $M_w$ ), and the dispersity index ( $D$ ) of the PSS. We hereon refer to the PSS samples used for tissue experimentation by their  $M_w$  (PSS-11kDa, PSS-20kDa and PSS-65kDa). We also characterized the same ( $M_n$ ,  $M_w$  and  $D$ ) for a CS reference standard

(Chondroitin Sulfate A sodium salt, 90+% purity, ThermoFisher Scientific), referred to as CS-A throughout this paper. All GPC traces are provided in the Supporting Information (**Figure S3**).

**3.4. Cartilage Explant Harvesting.** 6 mm full-thickness cartilage explants were harvested from freshly sacrificed bovine (*Bos taurus* or cattle) metacarpal phalangeal joints (Sudlersville Meat Locker, MD) with a cylindrical biopsy punch with aseptic techniques. Animals were slaughtered for reasons unrelated to this study. Only joints without evidence of gross macroscopic defects were dissected. Explants were rinsed thoroughly with phosphate buffered saline or PBS (1X PBS, RMBio). Explants were then transferred to a standard 12-well plate (1 explant/well with 2 mL working volume) for subsequent experimentation.

**3.5. Supernatant PSS Concentration Quantification.** Frozen supernatant aliquots were thawed following each experiment, and PSS supernatant concentrations were quantified using UV-Vis spectroscopy on a microplate reader (FLUOstar Omega Microplate Reader, BMG Labtech) at  $\lambda = 225$  nm. UV transparent 96-well plates were used (Santa Cruz Biotechnology) to reduce background absorbance at  $\lambda = 225$  nm (**Figure S4A**). Calibration curves of each PSS (PSS-11kDa, PSS-20kDa and PSS-65 kDa) are provided in the Supporting Information (**Figure S4B**).

**3.6. Safranin O Histological Staining.** All cartilage explants were fixed in 10% neutral buffered formalin (NBF) at 25 °C for 24 h, routinely processed for paraffin embedding, and sectioning at 4  $\mu$ m thickness onto charged slides, prior to staining with Safranin O/Fast Green (Safranin O Cartilage Staining Kit, American MasterTech). Detailed tissue processing and staining protocols have been provided in the Supporting Information. To standardize staining technique, all slides were stained simultaneously along with respective contemporaneously run controls. Images of

the stained slides were taken on a Zeiss Axiovert 200M microscope and then batch analyzed using automated scripts in MATLAB (Mathworks).

**3.7. Conditions for CS-A Diffusion at 4 °C.** Cartilage explants were randomly assigned to one of three experimental groups: 1) positive control or healthy cartilage, 2) negative control or GAG digested cartilage and 3) CS-A treated samples.

Positive control samples were incubated in PBS for 4 h at 37 °C, and then in PBS for 24 h at 4 °C, after which they were fixed in NBF for tissue fixation and histological staining. These positive control samples serve as an internal Safranin O staining control. Negative control samples were incubated in 1X 0.5% trypsin-EDTA (10X 0.5% trypsin-EDTA, ThermoFisher Scientific) in PBS for 3 h at 37 °C, as based on a previously described protocol for GAG digestion<sup>33,62</sup>. Samples were then incubated in PBS for 1 h at 37 °C, after which they were fixed in NBF. CS-A treated samples were incubated in 0.5% trypsin-EDTA for 3 h at 37 °C, in PBS for 1 h at 37 °C, and then in CS-A solution for 24 h at 4 °C, after which they were fixed in NBF. CS-A solution was prepared by dissolving 50 mg/mL of the reference CS-A standard in PBS.

**3.8. Conditions for PSS Unsteady State Diffusion at 37 °C.** Cartilage explants were randomly assigned to one of the eleven experimental groups listed in **Table 1**.

**Table 1.** Experimental Groups for PSS Unsteady State Diffusion Experiment.

Treatment	Groups
Control	Positive, Negative
PSS-11kDa Treated	5 min PSS incubation, 15 min PSS incubation, 60 min PSS incubation
PSS-20kDa Treated	5 min PSS incubation, 15 min PSS incubation, 60 min PSS incubation
PSS-65kDa Treated	5 min PSS incubation, 15 min PSS incubation, 60 min PSS incubation

Positive control samples were incubated in PBS for 4 h at 37 °C, after which they were placed in NBF for tissue fixation and histological staining. Negative control samples were

incubated in 0.5% trypsin-EDTA for 3 h at 37 °C, in PBS for 1 h at 37 °C, and then in PBS for 24 h at 4 °C, after which they were fixed in NBF. The PSS treated samples were first digested with 0.5% trypsin-EDTA in PBS for 3 h at 37 °C and then incubated in PBS for 1 h at 37 °C. Cartilage samples were finally incubated in the respective PSS solution (50 mg/mL PSS-11kDa, PSS-20kDa or PSS-65kDa in PBS) for the respective incubation time (5 min, 15 min or 60 min) at 37 °C. After PSS incubation, cartilage explants were immediately fixed in NBF.

**3.9. Conditions for PSS Static Desorption at 4 °C.** Cartilage explants were randomly assigned to one of five experimental groups: 1) positive control or healthy cartilage, 2) negative control or GAG digested cartilage, 3) PSS-11kDa treated samples, 4) PSS-20kDa treated samples and 5) PSS-65kDa treated samples.

Positive control samples were incubated in PBS for 4 h at 37 °C, and then in PBS for 24 h at 4 °C, after which they were fixed in NBF for tissue fixation and histological staining. Negative control samples were incubated in 0.5% trypsin-EDTA for 3 h at 37 °C, in PBS for 1 h at 37 °C, and then in PBS for 24 h at 4 °C, after which they were fixed in NBF. PSS treated samples (PSS-11kDa, PSS-20kDa and PSS-65kDa) were first incubated in 0.5% trypsin-EDTA in PBS for 3 h at 37 °C, in PBS for 1 h at 37 °C, and then in the respective PSS solution (50 mg/mL PSS in PBS) for 24 h at 4 °C. The PSS treated samples were finally incubated in four subsequent 24 h PBS rinses. Aliquots of supernatant (2 mL) were removed every 24 h and frozen at – 20 °C for later UV-Vis spectroscopy quantification, and the bathing solution was replaced with fresh PBS every day. Parallely, PSS treated explants were removed at Days 0 and 4, and then fixed in NBF.

**3.10. Conditions for PSS-65kDa Desorption Under Loading at 25 °C.** 6 mm full-thickness cartilage explants were harvested aseptically, using a cylindrical biopsy punch, from freshly

sacrificed bovine (*Bubalus bubalis* or water buffalo) metacarpal phalangeal joints (Sudlersville Meat Locker, MD). Water buffalo was used due to joint availability, however controls were appropriately used for comparison between groups within the experiment. Animals were slaughtered for reasons unrelated to this study. Only joints without gross macroscopic defects were dissected. Explant thicknesses were then measured using a caliper. Explants were then rinsed well with PBS immediately after harvest and transferred to a standard 12-well plate (1 explant/well with 2 mL working volume). Cartilage explants were randomly assigned to one of four experimental groups: 1) positive control or healthy cartilage, 2) negative control or GAG digested cartilage, 3) PSS-65kDa treated samples that were not loaded, and 4) PSS-65kDa treated samples that were loaded.

Positive control explants were incubated in PBS for 4 h at 37 °C, and then in PBS for 24 h at 4 °C, after which they were fixed in NBF for tissue fixation and histological staining. Negative control samples were incubated in 0.5% trypsin-EDTA for 3 h at 37 °C, in PBS for 1 h at 37 °C, and then in PBS for 24 h at 4 °C, after which they were fixed in NBF. PSS-65kDa treated samples were first incubated in 0.5% trypsin-EDTA in PBS for 3 h at 37 °C, in PBS for 1 h at 37 °C, and then in PSS solution (50 mg/mL PSS-65kDa in PBS) for 24 h at 4 °C.

Following PSS-65kDa diffusion, loaded samples were placed with the superficial side facing up and underwent 5, 15, 30 and 60 unconfined compression cycles with a target force of approximately 3 N compression was performed on a custom mechanical setup, where the indenter was fixed with a linear motor (Newmark Systems Inc.) and a sensitive force sensor (FUTEK, 250 g). Additionally, the indenter was fitted with a 3D-printed indenter tip with a square cross section (10 mm × 10 mm). Aliquots of supernatant (2 mL) were removed after every loading period (5, 15, 30 and 60 cycles) and frozen at –20 °C for later UV-Vis

spectroscopy quantification, and the bathing solution was replaced with fresh PBS. Parallely, the unloaded group underwent static desorption for the same duration of time as the loaded samples and similarly, aliquots of supernatant (2 mL) were removed and frozen at  $-20\text{ }^{\circ}\text{C}$  for later UV-Vis spectroscopy quantification. All PSS-65kDa treated cartilage explants (both loaded and not loaded) were removed following the experiment, and then fixed in NBF.

**3.11. Polymer SAXS Characterization.** Small-angle X-ray scattering (SAXS) measurements were performed at the LiX (16-ID) beamline of the National Synchrotron Light Source NSLS-II, Brookhaven National Laboratory (New York, US). Two detectors, Pilatus3X 1M and Pilatus3X 900K were placed with sample-to-detector distances of 3.566m and 0.315m, respectively. The combination of the two detectors covered a scattering range of  $q$  from around  $0.007\text{ } \text{\AA}^{-1}$  to  $2\text{ } \text{\AA}^{-1}$ . Sample solutions were prepared with a concentration of 50 mg/mL in 1X PBS (CS-A, PSS-11kDa, PSS-20kDa and PSS-65kDa) and loaded into an 8-cell flat window holder. All the samples were measured with an acquisition time of 1 second per frame for a total of 20 frames on different spots of the sample cell. The scattering of the empty cells and cells filled with PBS were also measured to be used for background subtraction. Background subtraction and averaging of the data were performed using JupyterHub, which was provided by Brookhaven National Laboratory.

**3.12. Safranin O – Polyanion Complex Absorption Spectra.** Standard solutions of CS-A, PSS-11kDa, PSS-20kDa and PSS-65kDa were prepared by dissolving the respective polyanions in DI water at the following concentrations: 0 mg/mL (DI water only), 0.001 mg/mL, 0.01 mg/mL, 0.1 mg/mL, 1 mg/mL and 10 mg/mL. A 1:200 Safranin O solution was prepared by diluting Safranin O stock solution (Safranin O Cartilage Staining Kit, American MasterTech) with DI water to ensure the absorbance spectrum remains below 1, as shown in the Supporting

Information (**Figure S5**). In a flat-bottom polystyrene 96-well plate, 50  $\mu\text{L}$  of each standard was mixed with 100  $\mu\text{L}$  of the 1:200 Safranin O solution and absorbance spectrums were captured from 400 nm to 600 nm using a microplate reader (FLUOstar Omega Microplate Reader, BMG Labtech) after 1 min of shaking. Each standard concentration was run as a triplicate within each group.

**3.13. Statistical Analysis.** All statistical analyses was performed with the JMP Pro 16 software (JMP Statistical Discovery LLC). Statistical significance was determined using non-parametric tests or parametric tests (after confirmation of normality and homogeneity of variance) and the specific statistical tests used are specified throughout.

## 4. RESULTS AND DISCUSSION

**4.1. Characterizing Polymer Molecular Weights.** A summary of molecular weight characterization of the polymers is shown in **Table 2**. While PSS-65kDa has a similar  $M_w$  as CS-A, it has a larger  $D$  than CS-A, which instead has a  $D$  more comparable to that of PSS-11kDa and PSS-20kDa.

**Table 2.** Polymer Molecular Weight and Dispersity.

Polymer	$M_w$ (kDa)	$M_n$ (kDa)	$D = M_w / M_n$
CS-A	60.7	41.7	1.5
<b>PSS-11kDa</b>	10.8	7.5	1.5
<b>PSS-20kDa</b>	20.4	13.0	1.6
<b>PSS-65kDa</b>	64.6	26.7	2.4
Porcine CS <sup>26,63–65</sup>	13.7 – 18.7	9.0 – 13.0	1.35 – 1.65
Bovine CS <sup>26,63–65</sup>	20.0 – 26.0	10.0 – 15.0	1.80 – 2.20
Shark CS <sup>26,63–65</sup>	64.2 – 70.2	20.5 – 26.0	2.50 – 3.10

Example for PSS-11kDa of the naming convention used in this article: 11 kDa refers to 11  $\text{kg mol}^{-1}$ , the weight average molecular weight of the PSSNa polymer. Bolded polymers indicate compounds tested in this study.

Biologically-derived CS has molecular weights in the range of 50 – 100 kDa *in vivo*, however after the extraction and purification process, the molecular weights of CS can drastically vary depending on the animal source the CS is sourced from.<sup>14</sup> For example, Volpi and co-workers found that commercially available CS preparations (sourced from porcine, chicken, bovine, shark and skate) had  $M_w$  ranging from approximately 10 kDa – 70 kDa.<sup>26,66</sup> This range from biologically-derived sources is covered by our CS-A reference and our PSS variants (PSS-11kDa, PSS-20kDa and PSS-65kDa). Another important parameter in characterizing the molecular mass is the dispersity ( $D$ ). Volpi and co-workers found that  $D$  ranged from 1.35 – 1.65 in porcine CS, from 1.80 – 2.20 in bovine CS, and from 2.50 – 3.10 in shark CS<sup>26,63–65</sup> (**Table 2**), which are the three main animal sources of commercial CS preparations<sup>14</sup>. Hence, PSS-11kDa and PSS-20kDa have comparable overall mass parameters ( $M_n$ ,  $M_w$  and  $D$ ) to bovine and porcine CS while PSS-65kDa is comparable to shark CS samples<sup>26</sup>. We note that the CS-A reference standard we used here is highly purified chondroitin sulfate A (90+% purity, ThermoFisher Scientific), since most commercial CS mixtures contain large amounts of other contaminants like dermatan sulfate<sup>24</sup>. We specifically chose to use chondroitin sulfate A since it is the predominant structural form in isolated CS<sup>26,66</sup>. Chondroitin sulfate A consists of a disaccharide unit, mono-sulfated at the 4<sup>th</sup> position of the *N*-acetyl-*D*-galactosamine. The structures of CS-A and PSS are provided for comparison in **Figure 1**.

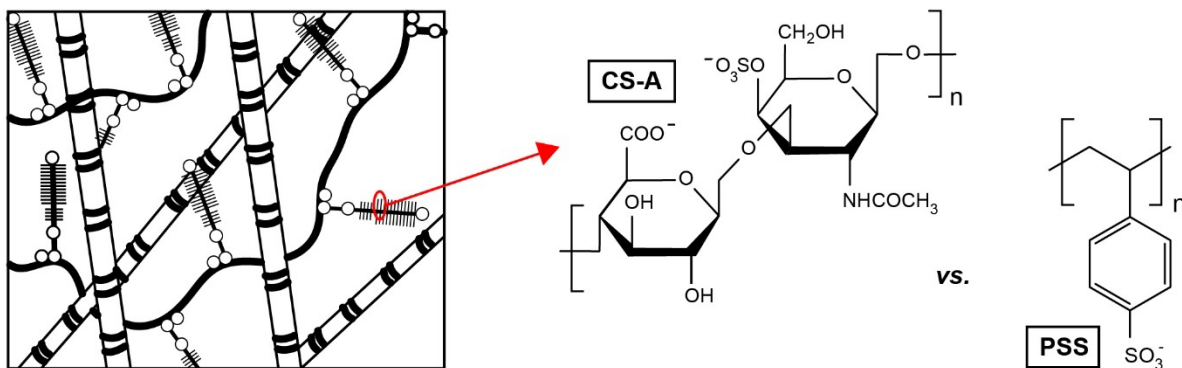


**Figure 1.** Structure of cartilage extracellular matrix and chemical structures of CS-A (GAG) versus PSS. CS-A = chondroitin sulfate A, GAG = glycosaminoglycan, PSS = poly(styrene sulfonate).

**4.2. CS-A Diffusion at 4 °C in Cartilage as a Reference.** To visualize the spatial distribution of supplemental CS-A within the cartilage explants, we utilized Safranin O, an established histochemical stain used in musculoskeletal research to quantitatively stain for the presence of polyanionic content in cartilage tissue.<sup>67</sup> More specifically, Safranin O itself is a cationic dye that preferentially binds with anionic groups present on native sulfated GAGs in cartilage with minimal off-target binding to collagen.<sup>68</sup> Safranin O is used in conjunction with the counterstain Fast Green, such that blue staining by Fast Green traditionally indicates GAG negative areas and purple-to-red staining by Safranin O traditionally indicates GAG positive areas.

Full thickness cartilage explants were subjected to a trypsin digestion (or PBS in the case of the positive control group) to digest all proteoglycans from the tissue, after which explants were subjected to a 50 mg/mL CS-A diffusion at 4 °C (or PBS alone in the case of the controls) for 24 h (**Figure 2A**, full experimental conditions listed in Methods). CS-A diffusion was performed for 24 h since the *in vivo* clearance rate of large molecules in the synovium to the plasma is  $t_{1/2} = 23.6$  h<sup>69</sup>. CS-A diffusion was also performed at 4 °C, similar to previous studies on cartilage solute diffusion<sup>70</sup>, to reduce enzymatic degradation and excess trypsin digestion during the overnight diffusion period. (Trypsin has minimal activity at low temperatures.<sup>71</sup>). The common protease inhibitor cocktail (5 mM benzamidine hydrochloride (BHCl) and 5 mM ethylenediaminetetraacetic acid (EDTA))<sup>72</sup> used in cartilage studies was not used here since there is an overlap in the absorbance between PSS and BHCl at the  $\lambda = 225$  nm wavelength we use to quantify PSS concentrations in supernatant (**Figure S4A** insert). As a result, we chose to lower

the temperature, instead of using external protease inhibitors, to reduce background enzymatic activity. CS-A diffusion was also performed at 4 °C, in alignment with previous cartilage explant studies, which showed that 50 mg/mL CS diffusion at 4 °C for 24 h failed to improve fluid load support in GAG depleted cartilage<sup>20</sup>. Following CS-A diffusion, cartilage explants were then fixed and stained with Safranin O after the 24 h diffusion period. The respective Safranin O staining areas were finally quantified by using an automated image processing script (**Figure 2B & C**). Safranin O staining intensity is relative<sup>68</sup> and staining between samples was performed with the same stain batch, concentration, and duration so that all imaging of stains could be accurately compared against the negative and positive controls within the experiment.

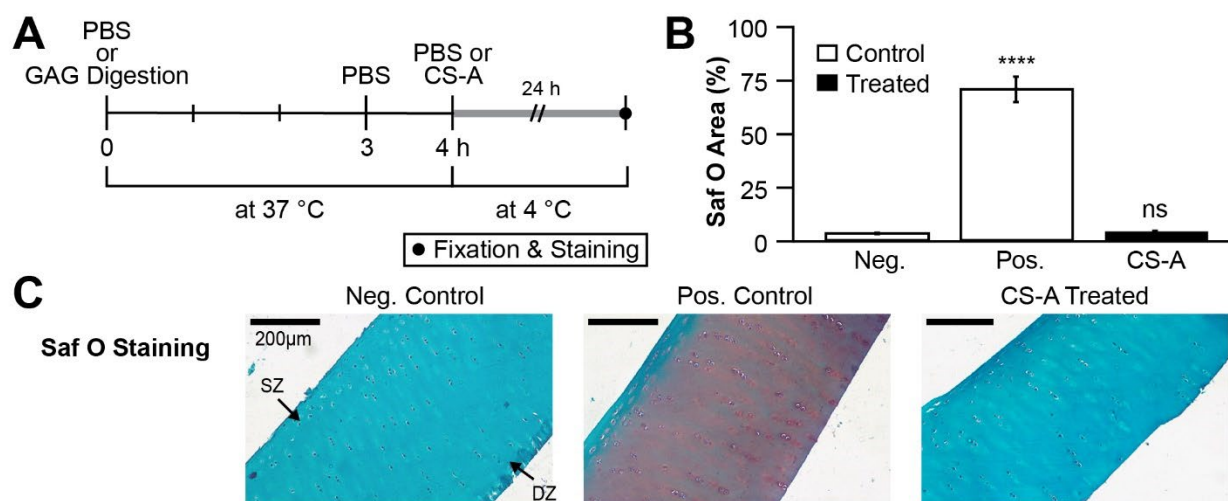


**Figure 2.** CS-A diffusion at 4 °C. PBS = phosphate buffered saline, CS-A = chondroitin sulfate  
A, GAG = glycosaminoglycan, SZ = superficial zone, DZ = deep zone. **(A)** Timeline of diffusion experiment. Controls and CS-A (50 mg/mL) treated explants were fixed and stained immediately following the 24 h diffusion period. **(B)** Average Safranin O area percentage, as quantified from Safranin O staining. Error bars indicate standard error of the mean.  $n = 15$  images taken over 3 explants per group. Statistical significance compared against negative control as determined with a Steel-Dwass nonparametric multiple comparisons test (ns = not significant, \*\*\*\*  $p < 0.0001$ ).

(C) Photomicrographs of Safranin O staining. All images oriented the same way with respect to cartilage zones.

**Figure 2C** shows that the trypsin digestion removed all GAG content from the tissue (negative control). While this differs from the physiological scenario during osteoarthritis where GAG loss is progressive from the superficial side in naturally occurring OA<sup>67</sup>, simulating partial digestion of proteoglycans using enzymes like trypsin can be highly variable<sup>73</sup>. This variability in GAG digestion would negatively impact our goals for establishing diffusive and kinetic properties of the polyanions we test here (e.g. CS-A). Furthermore, variations in native GAG concentrations have been shown to have a significant effect on charged solute diffusion in cartilage due to electrostatic interactions with the tissue.<sup>44,50</sup> Thus, we opted for complete proteoglycan digestion. This also further simplifies tracking of the absorbed polyanions through the cartilage explant sample since Safranin O does not exhibit any specificity against the native GAG versus externally introduced polyanions (e.g. CS-A)<sup>74</sup>.

Overall, **Figure 2** shows that the CS-A treated samples resulted in insignificant Safranin O staining and is comparable to that of the negative control group which had complete removal of GAGs. A repeat of the experiment on a separate dissection day demonstrates comparable results (**Figure S6**). It is likely that CS did not diffuse significantly enough into the tissue to properly integrate within the tissue and be captured by the Safranin O staining or it diffused out too quickly during solution exchanges from routine histology processing steps<sup>68</sup>. Regardless, our experiments with CS support findings that CS may not provide effective therapeutic benefit in cartilage, at least for the purpose of restoring osmotic responsiveness or load support in GAG depleted cartilage.<sup>20,21</sup> Similar conclusions were reached by Katta et al. who found no osmotic and fluid load support benefit from CS to cartilage.<sup>20</sup> In addition, Bian et al. found evidence for

some CS mechanical benefit, but only at exceeding high concentration of 100 mg/mL, which caused other adverse effects.<sup>21</sup> However, these previous studies had not performed Safranin O staining after CS treatment to indicate spatial distribution of supplemental charge in the bulk matrix, as we perform here. Our Safranin O stains (**Figure 2**) explain the lack of mechanical efficacy administered by a CS treatment.

**4.3. PSS Diffusion at 37 °C and Determination of Diffusion Coefficients.** We determined effective diffusion coefficients for PSS (PSS-11kDa, PSS-20kDa and PSS-65kDa) through an unsteady state diffusion experiment. Full thickness cartilage explants were subjected to a trypsin digestion, after which explants were subjected to 50 mg/mL PSS diffusion at 37 °C for either 5 min, 15 min or 60 min (**Figure 3A**). Diffusion was performed at 37 °C so we could determine diffusion coefficients based on molecular kinetics at physiological conditions. Negative and positive controls were exposed to PBS alone for 60 min. Explants were then fixed and stained with Safranin O before the PSS diffusion period for the control groups or immediately after each diffusion timepoint for the PSS treated samples. Cartilage is known to be anisotropic, and histology was performed in an orientation that allowed for examination of the superficial zone through deep layers of cartilage so that PSS zone-dependent diffusion coefficients could be determined. While Safranin O has not been established to bind to PSS before in histochemical tissue staining, we expected and confirm here that the cationic stain would be broadly applicable to polyanions like PSS.

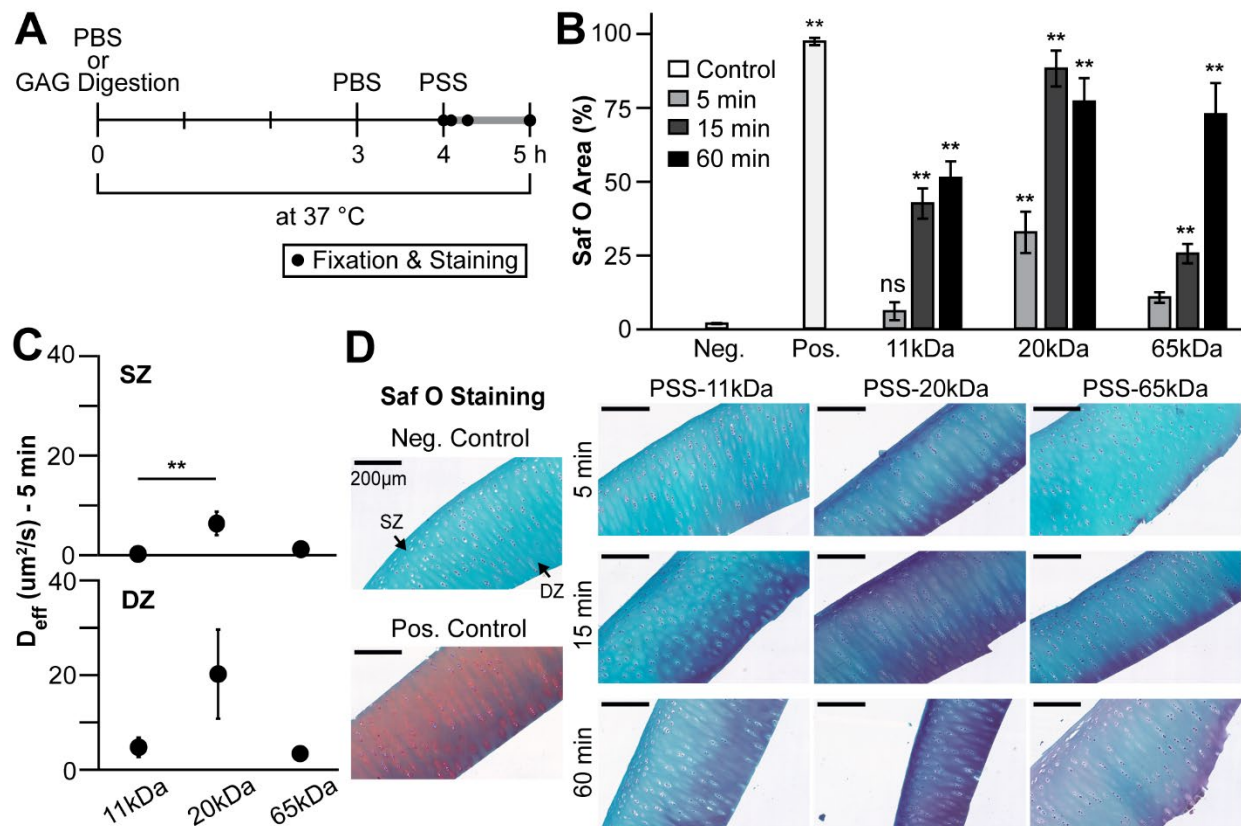


**Figure 3.** PSS unsteady state diffusion over range (PSS-11kDa, PSS-20kDa and PSS-65kDa) at 37 °C. PBS = phosphate buffered saline, PSS = poly(styrene sulfonate), GAG = glycosaminoglycan, SZ = superficial zone, DZ = deep zone. **(A)** Timeline of unsteady-state diffusion experiment. Controls were fixed and stained immediately at  $t = 4$  h. PSS treated samples were fixed and stained after  $t = 5$  min,  $t = 15$  min and  $t = 60$  min incubation in PSS solution (50 mg/mL). **(B)** Average Safranin O area percentage, as quantified from Safranin O staining. Error bars indicate standard error of the mean.  $n = 10$  images taken over 2 explants per group. Statistical significance compared against negative control as determined with a Steel-Dwass nonparametric multiple comparisons test (ns = not significant, \*  $p < 0.05$ , \*\*  $p < 0.01$ ). **(C)** Average unsteady diffusion coefficients calculated at  $t = 5$  min from intensities of Safranin O staining. Error bars indicate standard error of the mean.  $n = 10$  images taken over 2 explants per group. Statistical significance, within each zone, determined with a Steel-Dwass nonparametric

multiple comparisons test (\*\*  $p < 0.01$ ). **(D)** Photomicrographs of Safranin O staining. All images oriented the same way with respect to cartilage zones.

We quantified the respective Safranin O staining areas using an automated image processing script (**Figure 3B**) in MATLAB, based on a previously used procedure<sup>75</sup>. All three PSS diffused rapidly through the tissue at 37 °C and within 60 min, provided at least 50% area coverage. Nonspecific electrostatic interactions here drive weak and reversible binding of the charged PSS molecules within cartilage and as a result, charged solutes will continue to diffuse throughout the full thickness of the tissue while still exhibiting high tissue residence times.<sup>50</sup> This can be seen from **Figure 3B** where more PSS (for PSS-11kDa, PSS-20kDa and PSS-65kDa) saturates the tissue as the diffusion time is increased. Furthermore, the Safranin O photomicrographs demonstrate that the PSS treatments, unlike CS-A, result in positive staining for polyanionic content within the explants even after the solution exchanges that occur during routine histological processing steps.

Effective diffusion coefficients for the three PSS (PSS-11kDa, PSS-20kDa and PSS-65kDa) were then calculated from the overall staining intensities of the Safranin O photomicrographs at  $t = 5$  min (**Figure 3C & D**). This is justifiable because Safranin O broadly binds to polyanions in an orthochromatic form on permanently mounted histological tissue sections and as a result, the staining intensity should be proportional or stoichiometric to the polyanionic concentration within the tissue.<sup>74</sup> As such, the Safranin O staining intensities were fit to the solution of Fick's second law for a semi-infinite medium to calculate for the respective diffusion coefficients:<sup>76</sup>

$$\frac{\partial C}{\partial t} = D \frac{\partial^2 C}{\partial x^2} \quad \text{Eqn. (1)}$$

$$C(x, t) = C_s * (1 - \operatorname{erf} \frac{x}{2\sqrt{Dt}}) \quad \text{Eqn. (2)}$$

Where  $D$  is the diffusion coefficient,  $C(x, t)$  is the concentration within the cartilage at any time,  $t$ , and depth,  $x$ . The boundary conditions are that the initial solute concentration within the tissue is zero, and that the boundary is kept at a constant concentration  $C_s$ . An example image analysis for obtaining diffusion profiles is given in the Supporting Information (**Figure S7**). It is important to note that the diffusion coefficients are effective diffusion coefficients since there may be some loss of the PSS during the routine histological steps. However, calculation of effective solute diffusion coefficients after tissue explant embedding and sectioning has been previously reported for fluorescently labelled solute transport in cartilage.<sup>77</sup>

The Safranin O stains demonstrate that PSS-20kDa diffuses faster than PSS-11kDa and PSS-65kDa from both the superficial zone (SZ) and deep zone (DZ) sides, We note, however, that this difference is only statistically significant in the SZ, but a similar trend does seem to occur in the DZ as well. This is an interesting result, since it has been generally shown that diffusivity is inversely proportional to the solute size.<sup>44</sup> However, much of cartilage solute transport has been studied on spherical solutes or neutral polymers (such as dextrans)<sup>44,45</sup>, and such a relationship has been primarily seen in the more ideal diffusion mechanics of spherical solutes<sup>45</sup>. While a similar trend may exist in linear solutes, the correlation between size and diffusivity is far weaker<sup>45</sup>, most probably due to the tortuous nature of the tissue and the flexibility of the solutes. Previous work on the transport of large flexible polyelectrolytes, specifically polyanionic molecules, in cartilage remains very limited and there is a significant need to better understand similar transport phenomena of such charged solutes.<sup>44,45</sup>

Furthermore, the Safranin O stains and **Table 3** demonstrate zonal dependence of the diffusion coefficients for all three PSS. It is well known that larger solutes exhibit nonuniform

diffusion profiles in cartilage and the local transport kinetics are a function of the tissue zone.<sup>44</sup> More specifically, Leddy et al. has shown that middle sized dextrans (40 kDa and 70 kDa) diffuse faster in the DZ compared to the SZ<sup>46</sup>, whereas Torzilli et al. has shown that removal of the SZ decreases diffusion of 10 kDa dextran indicating the zonal preference towards the SZ<sup>78</sup>. It is believed that these size zonal thresholds are a function of the innate structure of the cartilage (e.g. the collagen fibril orientation and zonal based compositional concentrations of the collagens versus proteoglycans)<sup>46</sup>. On the other hand, investigations into the interaction of large polyanionic solutes with the cartilage anisotropic structure remain limited. Here, all three PSS diffused faster from the DZ in as compared to the SZ in. This diffusion is most probably enhanced due to the complete digestion of the native proteoglycans through the trypsin digestion we performed, as it has been previously found that proteoglycan removal increases the diffusion coefficient of similarly sized dextrans<sup>46</sup>. The DZ specifically has a large proteoglycan concentration in healthy cartilage. While the respective SZ and DZ diffusion coefficients for each of the three molecular weights were not found to be statistically different from each other, it has been shown previously that transient solute diffusion coefficients in cartilage can be highly variable<sup>77</sup>.

**Table 3.** Average Zonal-Based Effective Diffusion Coefficients for PSS

Polymer	$D_{\text{eff}}$ ( $\mu\text{m}^2/\text{s}$ ) from Superficial Zone	$D_{\text{eff}}$ ( $\mu\text{m}^2/\text{s}$ ) from Deep Zone
PSS-11kDa	$0.24 \pm 0.11 \mu\text{m}^2/\text{s}$	$4.74 \pm 2.04 \mu\text{m}^2/\text{s}$
PSS-20kDa	$6.35 \pm 2.37 \mu\text{m}^2/\text{s}$	$20.22 \pm 9.43 \mu\text{m}^2/\text{s}$
PSS-65kDa	$1.20 \pm 0.42 \mu\text{m}^2/\text{s}$	$3.41 \pm 1.06 \mu\text{m}^2/\text{s}$

Diffusion coefficients calculated from image analysis of Safranin-O staining (**Figure 3C & D**). Errors indicate standard error of the mean.  $n = 10$  images taken over 2 explants per group.

**4.4. PSS Desorption from Cartilage Under Static Conditions at 4 °C.** We measured solute retention for the three PSS formulations (PSS-11kDa, PSS-20kDa and PSS-65kDa) over a four-day period. Full thickness cartilage explants were subjected to a trypsin digestion (or PBS in

the case of the positive control group), after which explants were subjected to 50 mg/mL PSS diffusion at 4 °C for 24 h (or PBS alone in the case of the negative and positive controls). PSS treated explants were then placed in a PBS desorption bath for four days, where the solution was removed, saved and refreshed every 24 h (**Figure 4A**). Explants were incubated at 4 °C to compare diffusion results against the performance of CS-A (**Figure 2**) and to prevent background enzymatic activity that could affect solute kinetics in the tissue over the entire experimental timeline. In parallel, explants were fixed and stained with Safranin O on Day 0 and Day 4 (**Figure 4B**).

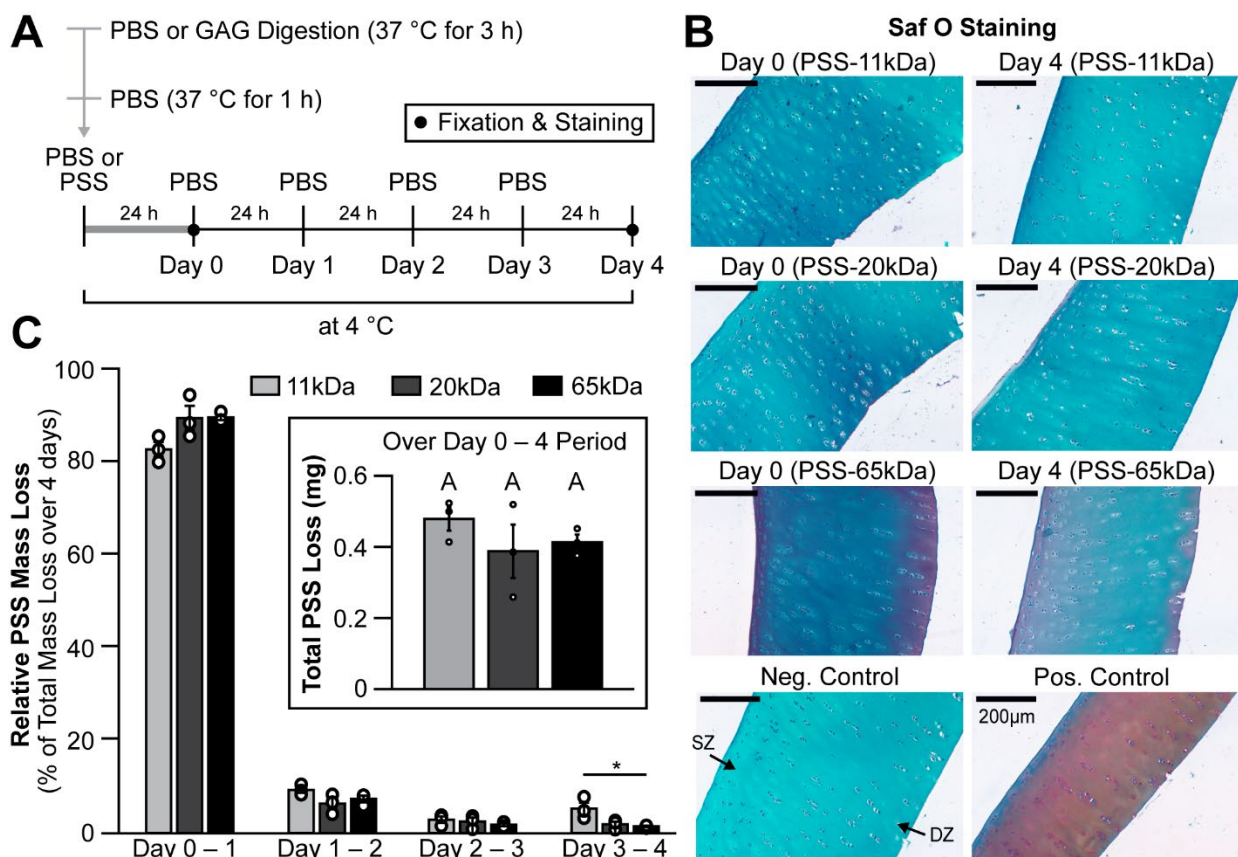


**Figure 4.** PSS (PSS-11kDa, PSS-20kDa and PSS-65kDa) diffusion and desorption at 4 °C.

PBS = phosphate buffered saline, PSS = poly(styrene sulfonate), GAG = glycosaminoglycan, SZ = superficial zone, DZ = deep zone. (**A**) Timeline of desorption experiment. Controls were fixed and stained at Day 0. PSS (50 mg/mL) treated samples were fixed and stained at Day 0 and

Day 4. **(B)** Photomicrographs of Safranin O staining. All images oriented the same way with respect to cartilage zones. **(C)** Average relative PSS mass loss (normalized against the total mass loss during the 4 day period) in supernatant over every 24 h PBS rinse, as quantified using UV-Vis spectroscopy at  $\lambda = 225$  nm. Error bars indicate standard error of the mean.  $n = 3$  cartilage explants per group. Statistical significance, within each group, determined with a Tukey's *post-hoc* multiple comparisons test (\*  $p < 0.05$ ). Total PSS mass loss (mg) over the entire 4-day period (Day 0 – 4) shown in the insert. Error bars indicate standard error of the mean.  $n = 3$  cartilage explants per group. Statistical significance determined with a Tukey's *post-hoc* multiple comparisons test (groups connected by the same letter are not significant at  $p$ -value of 0.05).

The Safranin O stains in **Figure 4B** demonstrate that a considerable portion of the PSS-65kDa that diffused into the tissue was still able to remain in the tissue even after the four 24 h PBS washes. These results demonstrate that PSS-65kDa is likely better at restoring fixed charge density over several days in GAG-depleted cartilage compared to the CS-A treatment (from **Figure 2**). The PSS-11kDa and PSS-20kDa that had diffused into the tissue on Day 0 were not significantly retained by the four-day period based on the Safranin O staining.

We also quantified the amount of PSS that diffused out of the tissue into the supernatant during every 24 h wash using UV-Vis spectroscopy (**Figure 4C**). PSS has been shown to have a maximum absorbance peak around  $\lambda = 225$  nm from its absorbance spectra.<sup>79</sup> PSS calibration curves for all three PSS (PSS-11kDa, PSS-20kDa and PSS-65kDa) are provided in **Figure S4B** and indicate linearity. Based on this, PSS concentrations were quantified at  $\lambda = 225$  nm and subsequently, the total mass losses over the entire four-day period were calculated. Mass loss was able to be determined because we had a volume of 2 mL per well at all points. From **Figure**

**4C**, there is diffusion of PSS from the explants during the desorption experiment. This solute loss is largest during Day 0 – 1 and decreases exponentially over each 24 h PBS rinse. However, the overall total PSS mass losses for the entire four-day period were not statistically different from each other over the three different polymer molecular weights (PSS-11kDa, PSS-20kDa and PSS-65kDa).

**4.5. PSS-65kDa Desorption from Cartilage Under Loading at 25 °C.** We measured the desorption of PSS-65kDa under unconfined compression loading. PSS-65kDa was chosen since this molecular weight had been shown to retain within the cartilage matrix for the longest duration out of the three PSS sizes tested (PSS-11kDa, PSS-20kDa and PSS-65kDa) (**Figure 4B**). Full thickness cartilage explants were subjected to a trypsin digestion (or PBS in the case of the positive control group), after which explants were subjected to 50 mg/mL PSS diffusion at 4 °C for 24 h (or PBS alone in the case of the controls). PSS treated explants were then assigned to two groups: one that underwent loading and the other that underwent static desorption for the same timeframe at 25 °C for a comparison. The not loaded samples serve as an internal control group for this experiment demonstrating PSS loss under static desorption since the loaded and not loaded samples were kept in the PBS bath for the same duration. Loaded samples were subjected to 5, 15, 30 and then 60 compression cycles in a PBS desorption bath, where the solution was removed, saved for analysis, and then refreshed upon every loading period (**Figure 5A**). Loading was standardized at a target compression force of approximately 3 N (or ~ 100 kPa) (**Figure S9**), in accordance with previous literature to simulate disruption of the superficial zone characteristic of early stage OA<sup>80</sup>. Loading was performed with an indenter tip which had a square cross section (10 mm × 10 mm) to ensure complete coverage over the 6 mm diameter explants. While it is common to load osteochondral plugs (full thickness cartilage with the

subchondral bone attached)<sup>80,81</sup>, we found that trypsin digestion of osteochondral plugs resulted in significant background absorbance at  $\lambda = 225$  nm, which would bias subsequent PSS quantification of the supernatant (**Figure S8**). As a result, we loaded full thickness cartilage biopsies (harvested without the subchondral bone) and the average tissue thickness of the loaded samples was found to be reasonably uniform ( $0.66 \pm 0.01$  mm), as measured with a caliper. In parallel, PSS treated explants control group (without load) underwent static desorption for the same durations as the loaded samples, and the corresponding solutions were also removed, saved for analysis, and refreshed. Explants were fixed and stained before the loading phase for the control groups or after the loading duration for all the PSS treated samples.

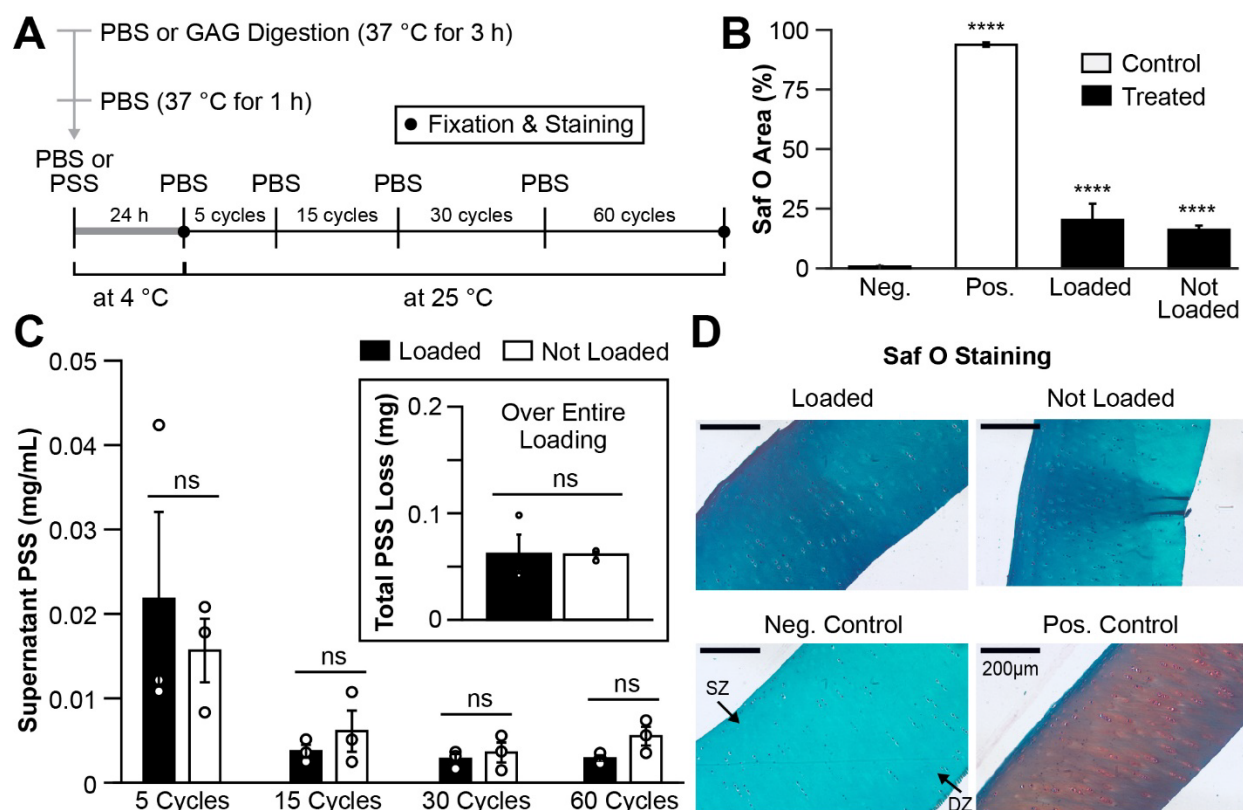


**Figure 5.** PSS-65kDa desorption under loading at 25 °C. PBS = phosphate buffered saline, PSS = poly(styrene sulfonate), GAG = glycosaminoglycan, SZ = superficial zone, DZ = deep zone.

(A) Timeline of desorption experiment. Controls were fixed and stained after the 24 h diffusion

period. PSS treated (50 mg/mL PSS-65kDa, loaded and unloaded) samples were fixed and stained upon completion of the entire loading timeframe (after 60 cycles). **(B)** Average Safranin O area percentage, as quantified from Safranin O staining. Error bars indicate standard error of the mean.  $n = 15$  images taken over 3 explants per group. Statistical significance compared against negative control as determined with a Steel-Dwass nonparametric multiple comparisons test (\*\*\*\*  $p < 0.0001$ ). **(C)** Average PSS loss concentration (mg/mL) in supernatant over every loading period, as quantified using UV-Vis spectroscopy at  $\lambda = 225$  nm. Error bars indicate standard error of the mean.  $n = 3$  cartilage explants per group. Statistical significance, within each group, was determined with a t-test (ns = not significant). Total PSS mass loss (mg) over the entire loading period (5 – 60 cycles) shown in the insert. Error bars indicate standard error of the mean.  $n = 3$  cartilage explants per group. Statistical significance determined with a t-test (ns = not significant). **(D)** Photomicrographs of Safranin O staining. All images oriented the same way with respect to cartilage zones. Staining of the loaded and unloaded samples was performed after completion of the loading cycles, at the end of the experiment.

We quantified the respective Safranin O staining areas using the same automated image processing script (**Figure 5B**) as in earlier sections. The results demonstrate that while Safranin O staining area is significantly larger in the PSS treated samples when compared to the negative control group, there is no significant difference in staining areas between the loaded and not loaded samples. This demonstrates that the initial disruption of the superficial collagen network does not result in significant loss of the PSS-65kDa, which instead is able to retain within the matrix, likely due to its electrostatic properties or physical adhesion and entanglement. This outcome is further supported by studies that have shown that trypsin digestion does not change

or damage the collagen network.<sup>82,83</sup> We also quantified the amount of PSS that diffused out of the tissue into the supernatant during every 24 h wash using UV-Vis spectroscopy (**Figure 5C**). These results demonstrate similar trends in that there is not a significant difference between PSS loss between loaded and not loaded samples. Instead, PSS mass loss was comparable between the loaded and not loaded samples and the largest solute loss occurred during the first 5 cycle loading duration. This suggests that retention of PSS is driven by comparatively strong molecular interactions which override effects from external mechanical loading. Corresponding Safranin O stains also indicate that some PSS-65kDa remains within the tissue upon static desorption and upon loading (**Figure 5D**). While the compressive stresses tested here (~ 100 kPa) are lower than physiological contact stresses incurred *in vivo* during light to moderate activities (1 – 6 MPa)<sup>84,85</sup>, 100 kPa or 0.1 MPa (as we have performed here) is a commonly used contact stress in loading experiments for cartilage explant studies<sup>86</sup>. Since we are using full-thickness cartilage explants without the underlying subchondral bone and surrounding tissue, the associated strains might actually be quite similar or even higher than those experienced *in vivo*<sup>86</sup>. Nevertheless, our results suggest that some PSS is likely to remain within the cartilage matrix even after compressive loading at stresses characteristic of superficial zone collagen damage and early stage OA cartilage matrix softening<sup>80</sup>.

**4.6. Polymer Conformation Characterization.** Our running hypothesis is that PSS diffuses better into the tissue matrix than CS-A due to the improved compact nature of the PSS polymer. To compare the conformations of CS-A versus the three PSS (PSS-11kDa, PSS-20kDa and PSS-65kDa), we used solution-based small angle x-ray scattering (SAXS). Solutions of CS-A and PSS were prepared at 50 mg/mL in 1X PBS, in line with previous tissue experiments in **Figures 2 – 5**.

**Figure 6** shows the scattering intensities ( $I(q)$ ) of the polymers plotted against the scattering vector ( $q$ ). The low- $q$  regions reveal that there are deviations from the linear Guinier fit due to inter-particle interactions (**Figure S10**) and as a result, we were unable to calculate the radius of gyration,  $R_g$ , from the Guinier model. However, these deviations from nonlinearity are most probably a result of the high dispersities of the well-dissolved polymers and due to the concentration effects from the high solution concentrations used here (50 mg/mL).<sup>87,88</sup>

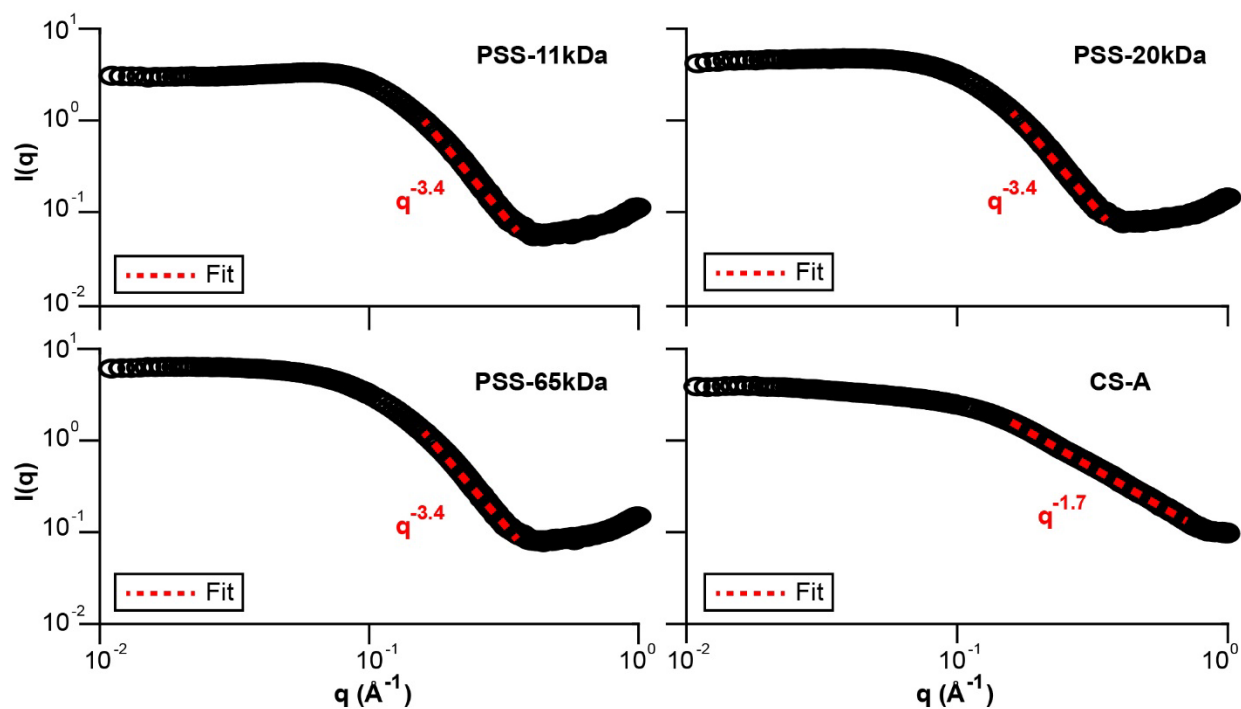


**Figure 6.** SAXS curves of CS-A versus PSS (PSS-11kDa, PSS-20kDa and PSS-65kDa), with curve fits using the Porod function. All four solutes were dissolved at a concentration of 50 mg/mL in 1X PBS. PSS = poly(styrene sulfonate), CS-A = chondroitin sulfate A.

We used the SAXS curves to investigate and compare the compactness of the polymer chains. The curves were first fitted with the Porod law as follows:

$$I \propto q^{-D} \quad \text{Eqn. (3)}$$

where  $I$  is the scattering intensity,  $q$  is the scattering vector, and  $D$  is the Porod exponent or the mass fractal of the polymer chain.<sup>89,90</sup> Linearization of **Eqn. (3)** and slope extraction of the regression fits have been presented in **Figure S11** and show strong linearity. Curve fits with the Porod law in **Figure 6** demonstrate that  $D_{\text{PSS}} = 3.4$  (for all three PSS molecular weights) and  $D_{\text{CS-A}} = 1.7$ . In the case of polymers, the Porod exponent is the inverse of the Flory exponent and as such,  $D = 3.4$  indicates a compact polymer system whereas  $D = 1.7$  indicates a swollen, extended polymer chain.<sup>88,89</sup>

The results show that PSS assumes a more compact structure in solution than CS-A does at the concentration of 50 mg/mL tested. This is further supported by the Kratky plots of the SAXS curves, as provided in **Figure S12**, which show that PSS solutions demonstrate a compact partially-folded conformation, whereas the CS-A assumes a swollen chain conformation in solution.<sup>88,89</sup> These results are in accordance with literature which show that CS exhibits a semi-rigid extended coil conformation with a persistence length on the order of 14 – 21 nm, translating to the increased stiffness present in aggrecan.<sup>91,92</sup>

**4.7. Safranin O – PSS Absorption Spectra.** To qualitatively compare the binding of the polyanions we tested here (eg. CS-A and PSS) with Safranin O, and to develop a colorimetric standard of stain color with PSS concentration, we measured the absorbance spectra of resulting dye – polyanion complexes in solution. We prepared a series of standard solution concentrations of CS-A and PSS (PSS-11kDa, PSS-20kDa and PSS-65kDa) in DI water and captured the absorption spectrums of the Safranin O dye – polyanion complexes using UV-Vis (**Figure 7**). Stock Safranin O stain was diluted by 1:200 using DI water to ensure that absorbance readings were in the working range of the microplate reader.

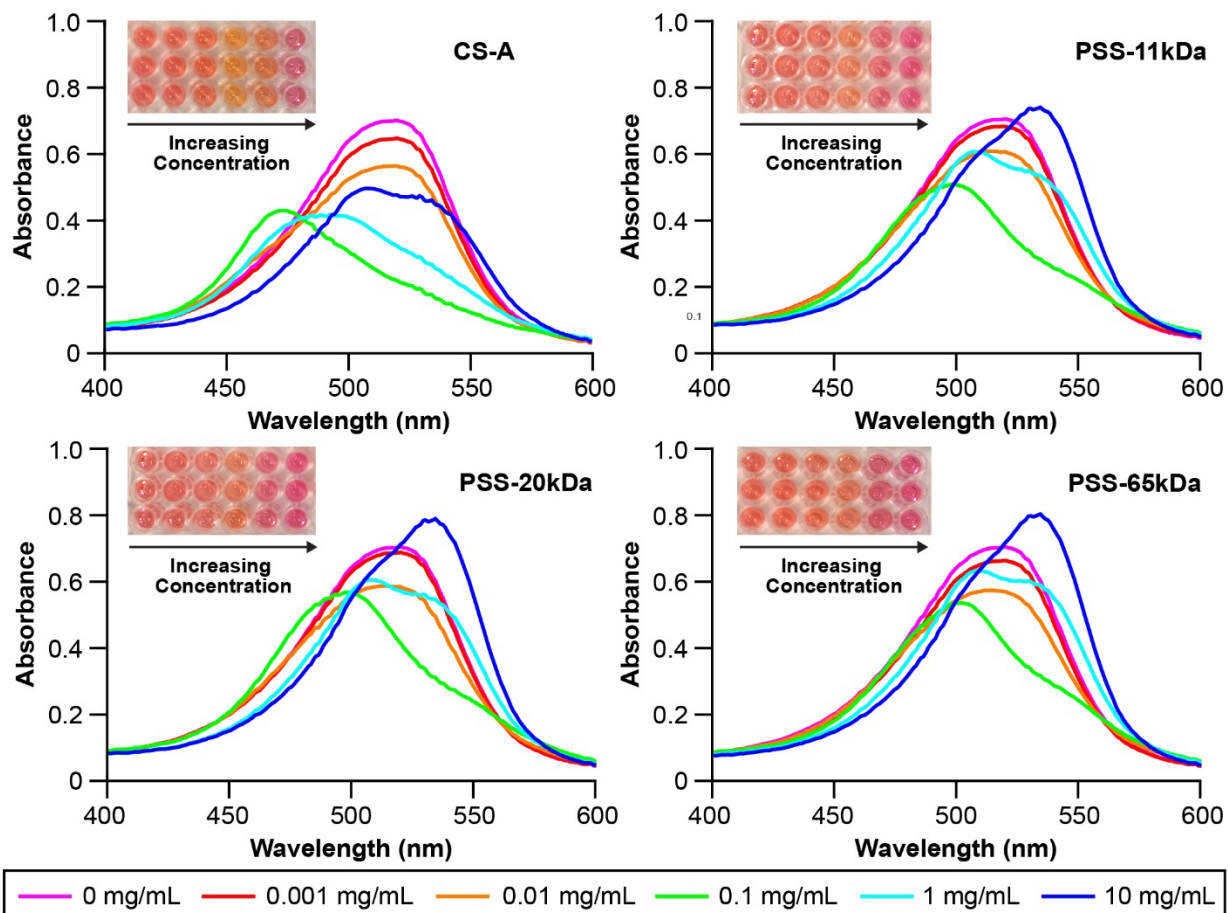


**Figure 7.** Safranin O – polyanion complex absorption spectra for CS-A, PSS-11kDa, PSS-20kDa and PSS-65kDa. Each absorbance spectrum line is the average of  $n = 3$  wells. Inserts illustrate solution color changes as the concentrations of the standard solutions are increased (from 0 mg/mL to 10 mg/mL from left to right).

From **Figure 7**, the 0 mg/mL (no added polyelectrolyte) absorption line demonstrates that the Safranin O dye has a maximum absorbance peak at  $\lambda = 519$  nm, which aligns with previous studies<sup>74</sup>. This peak, which occurs at  $\lambda = 519$  nm, is referred to as the orthochromatic peak and describes the color of the dye. Addition of CS-A and the three PSS (PSS-11kDa, PSS-20kDa and PSS-65kDa) to the dye solution first results in a depression of the orthochromatic (color intensity) absorbance maximum at polyanion concentrations of 0.001 mg/mL and 0.01 mg/mL as

seen in **Figure 7**. At a molecular level, this occurs due to adsorption of the cationic dye on the polyanions, occurring primarily through electrostatic interactions.<sup>74,93</sup> However, the changes in absorbance between the polyanions at each concentration were found to be not statistically significant from each other (**Table S2**).

When the concentrations exceeded 0.01 mg/mL, there were appearances of metachromatic (color shift) absorbance peaks, as seen in **Figure 7**. These color shifts occur due to dye – dye interactions between neighboring dye molecules bound to the polyanion from forced stacking of dye molecules along the molecular chain of the polyelectrolyte, thus inducing solution color change.<sup>74,93</sup> As a result, the ability of a polyanion to induce metachromasia is directly related to the inter-charge distance of that polyanion.<sup>74</sup> From **Figure 7**, it can be clearly seen that the wavelength shifts are more rapid with changes in concentration (e.g., occur at lower concentrations) with PSS as compared to with CS-A. For example, the metachromatic peak that occurs at  $\lambda \sim 507$  nm for 1 mg/mL PSS (PSS-11kDa, PSS-20kDa and PSS-65kDa) does not occur until 10 mg/mL CS-A. Wavelengths of each of the metachromatic absorbance peaks have been quantified in **Table S3**, and it was found that the wavelength shifts between CS-A and each PSS were statistically different from each other at each concentration (0.1 mg/mL, 1 mg/mL and 10 mg/mL).

The more rapid metachromatic shifts per concentration from PSS over CS-A indicates that PSS likely has a smaller inter-charge distance than CS-A. Combining these results with the SAXS conformation analysis of **Figure 6** demonstrates that PSS assumes a more compact conformation in solution than CS-A and, as a result, has a higher charge density as compared to CS-A. This structure of PSS is advantageous since the compact nature and increased charge density allows it to freely diffuse into and concentrate within the bulk matrix to provide

supplemental negative charge to the porous bulk matrix of GAG depleted cartilage as compared to CS-A does.

## 5. CONCLUSIONS

There is a critical need for GAG and proteoglycan analogues that help restore osmotic responsiveness in OA cartilage and rebuild impaired load-bearing tissue function via tissue hydration. Here, we demonstrated that PSS can be used to synthetically replace lost negative charge in cartilage (with complete GAG loss) as well as can be used to probe polyelectrolyte transport in cartilage. Effective diffusion coefficients of three different molecular weights of PSS (11kDa, 20kDa, and 65kDa) were determined through image analysis of Safranin O staining. It was found that PSS diffused faster from the deep zone side in than from the superficial zone side, regardless of the molecular weight of the PSS. Furthermore, PSS treated samples were able to retain a considerable amount of the supplemental charge even after 4 days and upon loading. In contrast, CS-A treated samples displayed little to no positive Safranin O staining and restoration of negative charge even on Day 0 of treatment.

We hypothesize that this improved solute retention exhibited by PSS over CS-A is due to the greater compactness and improved charge density of the PSS chain, as determined through solution-based SAXS. This conformation advantage helps the polyelectrolyte diffuse better into the tissue and possess a better binding capacity with the matrix, improving charge delivery and solute performance. Future work may include tracking polyelectrolyte diffusion kinetics through non-Newtonian solution baths (since synovial fluid is non-Newtonian in nature). Size dependent diffusion of polyanionic molecules can also be further investigated by tracking the diffusion of various polyelectrolytes through molecular labelling techniques. More broadly, our results open

avenues to using PSS functionalized proteoglycan replacements for restoring fixed charge density in GAG-depleted cartilage and could also be translated to similar hydrated tissue systems such as fibrocartilage and corneal tissue.

## 6. SUPPORTING INFORMATION

Supporting Information with the following: PSS sample preparation, Polymer GPC traces, PSS UV-Vis spectroscopy calibration curves, Tissue processing and staining protocols for histology, Safranin O absorption spectra, CS-A diffusion in cartilage, PSS diffusion coefficient analysis, Osteochondral plug background absorbances, Compressive loading cycles, SAXS data analysis, and quantification of Safranin O – Polyanion absorption spectra.

## 7. ACKNOWLEDGMENTS

This project was supported by the DCMR COBRE program, with a grant from the National Institute of General Medical Sciences and from the National Institutes of Health (NIH-NIGMS COBRE, P20GM139760) to C.D., L.V.K., J.P. and J.E. T.J.M. and J.P. acknowledge funding from NIGMS P20GM103446. W.X. and D.P. acknowledge funding from the NSF through the University of Delaware Materials Research Science and Engineering Center, DMR-2011824. A.N.Y. and L.V.K. thank the University of Delaware Research Foundation-Strategic Initiative (UDRF-SI) for seed funding.

Histology was performed by the DCMR Histology Core, University of Delaware, Newark, DE. SAXS experiments were performed at LiX beamline of the National Synchrotron Light Source II, a U.S. Department of Energy (DOE) Office of Science User Facility operated for the DOE Office of Science by Brookhaven National Laboratory under Contract No. DE-

SC0012704. The LiX beamline is part of the Center for BioMolecular Structure (CBMS) which is primarily supported by the National Institutes of Health, National Institute of General Medical Sciences (NIGMS) through a Center Core P30 Grant (P30GM133893), and by the DOE Office of Biological and Environmental Research (KP1607011). The authors would like to thank Dr. Kyla Ortved (University of Pennsylvania School of Veterinary Medicine) for her insights on OA. The authors would also like to thank Dr. David Martin (University of Delaware) and his lab for access to their microplate reader.

## 8. FINANCIAL STATEMENT

The authors declare the following competing financial interest(s): C.D., L.V.K., S.S., Q.B., A.N.Y., and V.S.D. are inventors on a U.S. provisional patent related to the use of synthetic polyelectrolytes for restoration of glycosaminoglycan and proteoglycan function in soft tissue.

## 9. AUTHOR CONTRIBUTIONS

S.S., L.V.K., and C.D. conceptualized the study, designed experiments and performed analysis. S.S., A.K., T.J.M., W.X., Q.B., and C.Y.L. performed experiments. S.S., A.K., V.S.D., A.N.Y., L.V.K., and C.D. wrote the original manuscript. C.D., L.V.K., J.B.E., J.P. and D.P. provided supervision and experimental guidance. All authors contributed to editing of the manuscript and have given approval to the final version of the manuscript.

## 10. REFERENCES

- (1) Hayes, A. J.; Melrose, J. Glycosaminoglycan and Proteoglycan Biotherapeutics in Articular Cartilage Protection and Repair Strategies: Novel Approaches to Visco-supplementation in Orthobiologics. *Adv. Ther.* **2019**, *2* (8), 1–39.

- <https://doi.org/10.1002/adtp.201900034>.
- (2) Arokoski, J. P. A.; Jurvelin, J. S.; Väättäin, U.; Helminen, H. J. Normal and Pathological Adaptations of Articular Cartilage to Joint Loading. *Scand. J. Med. Sci. Sports* **2000**, *10* (4), 186–198. <https://doi.org/10.1034/j.1600-0838.2000.010004186.x>.
  - (3) LU, X. L.; MOW, V. C. Biomechanics of Articular Cartilage and Determination of Material Properties. *Med. Sci. Sport. Exerc.* **2008**, *40* (2), 193–199. <https://doi.org/10.1249/mss.0b013e31815cb1fc>.
  - (4) Lai, W. M.; Hou, J. S.; Mow, V. C. A Triphasic Theory for the Swelling and Deformation Behaviors of Articular Cartilage. *J. Biomech. Eng.* **1991**, *113* (3), 245–258. <https://doi.org/10.1115/1.2894880>.
  - (5) Maroudas, A. Biophysical Chemistry of Cartilaginous Tissues with Special Reference to Solute and Fluid Transport1. *Biorheology* **1975**, *12* (3–4), 233–248. <https://doi.org/10.3233/BIR-1975-123-416>.
  - (6) Roughley, P. J.; Mort, J. S. The Role of Aggrecan in Normal and Osteoarthritic Cartilage. *J. Exp. Orthop.* **2014**, *1* (1), 8. <https://doi.org/10.1186/s40634-014-0008-7>.
  - (7) Favero, M.; Ramonda, R.; Goldring, M. B.; Goldring, S. R.; Punzi, L. Early Knee Osteoarthritis. *RMD Open* **2015**, *1* (Suppl 1), e000062. <https://doi.org/10.1136/rmdopen-2015-000062>.
  - (8) Pollard, T. C. B.; Gwilym, S. E.; Carr, A. J. The Assessment of Early Osteoarthritis. *J. Bone Joint Surg. Br.* **2008**, *90-B* (4), 411–421. <https://doi.org/10.1302/0301-620X.90B4.20284>.
  - (9) Nguyen, M.; Panitch, A. Proteoglycans and Proteoglycan Mimetics for Tissue Engineering. *Am. J. Physiol. Physiol.* **2022**, *322* (4), C754–C761.

- <https://doi.org/10.1152/ajpcell.00442.2021>.
- (10) Lee, D. W.; Banquy, X.; Israelachvili, J. N. Stick-Slip Friction and Wear of Articular Joints. *Proc. Natl. Acad. Sci.* **2013**, *110* (7). <https://doi.org/10.1073/pnas.1222470110>.
- (11) Athens, A. A.; Makris, E. A.; Hu, J. C. Induced Collagen Cross-Links Enhance Cartilage Integration. *PLoS One* **2013**, *8* (4), e60719. <https://doi.org/10.1371/journal.pone.0060719>.
- (12) Xu, R.; Wu, J.; Zheng, L.; Zhao, M. Undenatured Type II Collagen and Its Role in Improving Osteoarthritis. *Ageing Res. Rev.* **2023**, *91*, 102080. <https://doi.org/10.1016/j.arr.2023.102080>.
- (13) Hayes, A. J.; Melrose, J.; Phillips, E. R.; Haislup, B. D.; Bertha, N.; Lefchak, M.; Sincavage, J.; Prudnikova, K.; Shallop, B.; Mulcahey, M. K.; Marcolongo, M. S.; Rahimi, M.; Charmi, G.; Matyjaszewski, K.; Banquy, X.; Pietrasik, J.; Prudnikova, K.; Yucha, R. W.; Patel, P.; Kriete, A. S.; Han, L.; Penn, L. S.; Marcolongo, M. S.; Katta, J.; Jin, Z.; Ingham, E.; Fisher, J.; Moore, A. C.; Schrader, J. L.; Ulvila, J. J.; Burris, D. L.; DiDomenico, C. D.; Lintz, M.; Bonassar, L. J.; Sharma, S.; Vazquez-Portalatin, N.; Calve, S.; Panitch, A.; Phillips, E. R.; Prudnikova, K.; Bui, T.; Taylor, A. J.; Galindo, D. A.; Huneke, R. B.; Hou, J. S.; Mulcahey, M. K.; Marcolongo, M. S. Glycosaminoglycan and Proteoglycan Biotherapeutics in Articular Cartilage Protection and Repair Strategies: Novel Approaches to Visco-Supplementation in Orthobiologics. *Osteoarthr. Cartil.* **2019**, *2* (8), 31–50. <https://doi.org/10.1021/acs.biomac.7b00032>.
- (14) Henrotin, Y.; Mathy, M.; Sanchez, C.; Lambert, C. Chondroitin Sulfate in the Treatment of Osteoarthritis: From in Vitro Studies to Clinical Recommendations. *Ther. Adv. Musculoskelet. Dis.* **2010**, *2* (6), 335–348. <https://doi.org/10.1177/1759720X10383076>.
- (15) Henrotin, Y.; Marty, M.; Mobasher, A. What Is the Current Status of Chondroitin Sulfate

- and Glucosamine for the Treatment of Knee Osteoarthritis? *Maturitas* **2014**, *78* (3), 184–187. <https://doi.org/10.1016/j.maturitas.2014.04.015>.
- (16) Reginster, J.-Y.; Veronese, N. Highly Purified Chondroitin Sulfate: A Literature Review on Clinical Efficacy and Pharmacoeconomic Aspects in Osteoarthritis Treatment. *Aging Clin. Exp. Res.* **2021**, *33* (1), 37–47. <https://doi.org/10.1007/s40520-020-01643-8>.
- (17) Mazieres, B.; Hucher, M.; Zaim, M.; Garnero, P. Effect of Chondroitin Sulphate in Symptomatic Knee Osteoarthritis: A Multicentre, Randomised, Double-Blind, Placebo-Controlled Study. *Ann. Rheum. Dis.* **2007**, *66* (5), 639–645. <https://doi.org/10.1136/ard.2006.059899>.
- (18) Vangsness, C. T.; Spiker, W.; Erickson, J. A Review of Evidence-Based Medicine for Glucosamine and Chondroitin Sulfate Use in Knee Osteoarthritis. *Arthrosc. J. Arthrosc. Relat. Surg.* **2009**, *25* (1), 86–94. <https://doi.org/10.1016/j.arthro.2008.07.020>.
- (19) Distler, J.; Anguelouch, A. Evidence-based Practice: Review of Clinical Evidence on the Efficacy of Glucosamine and Chondroitin in the Treatment of Osteoarthritis. *J. Am. Acad. Nurse Pract.* **2006**, *18* (10), 487–493. <https://doi.org/10.1111/j.1745-7599.2006.00166.x>.
- (20) Katta, J.; Jin, Z.; Ingham, E.; Fisher, J. Chondroitin Sulphate: An Effective Joint Lubricant? *Osteoarthr. Cartil.* **2009**, *17* (8), 1001–1008. <https://doi.org/10.1016/j.joca.2009.02.010>.
- (21) Bian, L.; Kaplun, M.; Williams, D. Y.; Xu, D.; Ateshian, G. A.; Hung, C. T. Influence of Chondroitin Sulfate on the Biochemical, Mechanical and Frictional Properties of Cartilage Explants in Long-Term Culture. *J. Biomech.* **2009**, *42* (3), 286–290. <https://doi.org/10.1016/j.jbiomech.2008.10.032>.
- (22) da Cunha, A. L.; de Oliveira, L. G.; Maia, L. F.; de Oliveira, L. F. C.; Michelacci, Y. M.;

- de Aguiar, J. A. K. Pharmaceutical Grade Chondroitin Sulfate: Structural Analysis and Identification of Contaminants in Different Commercial Preparations. *Carbohydr. Polym.* **2015**, *134*, 300–308. <https://doi.org/10.1016/j.carbpol.2015.08.006>.
- (23) Restaino, O. F.; Finamore, R.; Diana, P.; Marseglia, M.; Vitiello, M.; Casillo, A.; Bedini, E.; Parrilli, M.; Corsaro, M. M.; Trifuoggi, M.; De Rosa, M.; Schiraldi, C. A Multi-Analytical Approach to Better Assess the Keratan Sulfate Contamination in Animal Origin Chondroitin Sulfate. *Anal. Chim. Acta* **2017**, *958*, 59–70. <https://doi.org/10.1016/j.aca.2016.12.005>.
- (24) Stellavato, A.; Restaino, O. F.; Vassallo, V.; Finamore, R.; Ruosi, C.; Cassese, E.; De Rosa, M.; Schiraldi, C. Comparative Analyses of Pharmaceuticals or Food Supplements Containing Chondroitin Sulfate: Are Their Bioactivities Equivalent? *Adv. Ther.* **2019**, *36* (11), 3221–3237. <https://doi.org/10.1007/s12325-019-01064-8>.
- (25) Theoharides, T. C. Dietary Supplements for Arthritis and Other Inflammatory Conditions: Key Role of Mast Cells and Benefit of Combining Anti-Inflammatory and Proteoglycan Products. *Eur. J. Inflamm.* **2003**, *1* (1), 1–8. <https://doi.org/10.1177/1721727X0300100102>.
- (26) Volpi, N. Analytical Aspects of Pharmaceutical Grade Chondroitin Sulfates. *J. Pharm. Sci.* **2007**, *96* (12), 3168–3180. <https://doi.org/10.1002/jps.20997>.
- (27) Ngadimin, K. D.; Stokes, A.; Gentile, P.; Ferreira, A. M. Biomimetic Hydrogels Designed for Cartilage Tissue Engineering. *Biomater. Sci.* **2021**, *9* (12), 4246–4259. <https://doi.org/10.1039/D0BM01852J>.
- (28) KWON, H. J.; HAN, Y. Chondroitin Sulfate-Based Biomaterials for Tissue Engineering. *TURKISH J. Biol.* **2016**, *40* (2), 290–299. <https://doi.org/10.3906/biy-1507-16>.

- (29) Shin, J.; Kang, E. H.; Choi, S.; Jeon, E. J.; Cho, J. H.; Kang, D.; Lee, H.; Yun, I. S.; Cho, S.-W. Tissue-Adhesive Chondroitin Sulfate Hydrogel for Cartilage Reconstruction. *ACS Biomater. Sci. Eng.* **2021**, *7* (9), 4230–4243. <https://doi.org/10.1021/acsbiomaterials.0c01414>.
- (30) Atwal, A.; Dale, T. P.; Snow, M.; Forsyth, N. R.; Davoodi, P. Injectable Hydrogels: An Emerging Therapeutic Strategy for Cartilage Regeneration. *Adv. Colloid Interface Sci.* **2023**, *321* (October), 103030. <https://doi.org/10.1016/j.cis.2023.103030>.
- (31) Bernhard, J. C.; Panitch, A. Synthesis and Characterization of an Aggrecan Mimic. *Acta Biomater.* **2012**, *8* (4), 1543–1550. <https://doi.org/10.1016/j.actbio.2011.12.029>.
- (32) Sharma, S.; Panitch, A.; Neu, C. P. Incorporation of an Aggrecan Mimic Prevents Proteolytic Degradation of Anisotropic Cartilage Analogs. *Acta Biomater.* **2013**, *9* (1), 4618–4625. <https://doi.org/10.1016/j.actbio.2012.08.041>.
- (33) Sharma, S.; Vazquez-Portalatin, N.; Calve, S.; Panitch, A. Biomimetic Molecules Lower Catabolic Expression and Prevent Chondroitin Sulfate Degradation in an Osteoarthritic Ex Vivo Model. *ACS Biomater. Sci. Eng.* **2016**, *2* (2), 241–250. <https://doi.org/10.1021/acsbiomaterials.5b00458>.
- (34) Prudnikova, K.; Yucha, R. W.; Patel, P.; Kriete, A. S.; Han, L.; Penn, L. S.; Marcolongo, M. S. Biomimetic Proteoglycans Mimic Macromolecular Architecture and Water Uptake of Natural Proteoglycans. *Biomacromolecules* **2017**, *18* (6), 1713–1723. <https://doi.org/10.1021/acs.biomac.7b00032>.
- (35) Phillips, E. R.; Haislup, B. D.; Bertha, N.; Lefchak, M.; Sincavage, J.; Prudnikova, K.; Shalloo, B.; Mulcahey, M. K.; Marcolongo, M. S. Biomimetic Proteoglycans Diffuse throughout Articular Cartilage and Localize within the Pericellular Matrix. *J. Biomed.*

- Mater. Res. - Part A* **2019**, *107* (9), 1977–1987. <https://doi.org/10.1002/jbm.a.36710>.
- (36) Phillips, E. R.; Prudnikova, K.; Bui, T.; Taylor, A. J.; Galindo, D. A.; Huneke, R. B.; Hou, J. S.; Mulcahey, M. K.; Marcolongo, M. S. Biomimetic Proteoglycans Can Molecularly Engineer Early Osteoarthritic Cartilage in Vivo. *J. Orthop. Res.* **2019**, *37* (2), 403–411. <https://doi.org/10.1002/jor.24193>.
- (37) Kahle, E. R.; Han, B.; Chandrasekaran, P.; Phillips, E. R.; Mulcahey, M. K.; Lu, X. L.; Marcolongo, M. S.; Han, L. Molecular Engineering of Pericellular Microniche via Biomimetic Proteoglycans Modulates Cell Mechanobiology. *ACS Nano* **2022**, *16* (1), 1220–1230. <https://doi.org/10.1021/acsnano.1c09015>.
- (38) FERRIS, D. J.; FRISBIE, D. D.; McILWRAITH, C. W.; KAWCAK, C. E. Current Joint Therapy Usage in Equine Practice: A Survey of Veterinarians 2009. *Equine Vet. J.* **2011**, *43* (5), 530–535. <https://doi.org/10.1111/j.2042-3306.2010.00324.x>.
- (39) Mertens, W. D.; MacLeod, J. N.; Fubini, S. L.; Vernier-Singer, M.; Nixon, A. J.; Todhunter, R. J. Polysulphated Glycosaminoglycans Modulate Transcription of Interleukin-1 $\beta$  Treated Chondrocytes in Monolayer Culture. *Vet. Comp. Orthop. Traumatol.* **2003**, *16* (02), 93–98. <https://doi.org/10.1055/s-0038-1632759>.
- (40) de Haan, J. J.; Beale, B. S.; Clemmons, R. M.; Clark, L. The Effects of Polysulfated Glycosaminoglycan (Adeqtiail®) on Activated Partial Thromboplastin Time, Prothrombin Time, Complete Blood Count, Biochemical Profile and Urinalysis in Cats. *Vet. Comp. Orthop. Traumatol.* **1994**, *07* (01), 77–81. <https://doi.org/10.1055/s-0038-1633046>.
- (41) Wonn, A. M.; Brooks, M. B.; Hu, H.; Gamble, K. C. HYPOCOAGULABILITY EFFECT OF ADEQUAN IN DOMESTIC CHICKENS (*GALLUS GALLUS*) AND CHILEAN FLAMINGOS (*PHOENICOPTERUS CHILENSIS*). *J. Zoo Wildl. Med.* **2022**, *53* (1).

<https://doi.org/10.1638/2021-0052>.

- (42) Mow, V. C.; Holmes, M. H.; Michael Lai, W. Fluid Transport and Mechanical Properties of Articular Cartilage: A Review. *J. Biomech.* **1984**, *17* (5), 377–394. [https://doi.org/10.1016/0021-9290\(84\)90031-9](https://doi.org/10.1016/0021-9290(84)90031-9).
- (43) Travascio, F.; Valladares-Prieto, S.; Jackson, A. R. Effects of Solute Size and Tissue Composition on Molecular and Macromolecular Diffusivity in Human Knee Cartilage. *Osteoarthr. Cartil. Open* **2020**, *2* (4), 100087. <https://doi.org/10.1016/j.ocarto.2020.100087>.
- (44) Didomenico, C. D.; Lintz, M.; Bonassar, L. J. Molecular Transport in Articular Cartilage - What Have We Learned from the Past 50 Years? *Nat. Rev. Rheumatol.* **2018**, *14* (7), 393–403. <https://doi.org/10.1038/s41584-018-0033-5>.
- (45) DiDomenico, C. D.; Bonassar, L. J. How Can 50 Years of Solute Transport Data in Articular Cartilage Inform the Design of Arthritis Therapeutics? *Osteoarthr. Cartil.* **2018**, *26* (11), 1438–1446. <https://doi.org/10.1016/j.joca.2018.07.006>.
- (46) Leddy, H. A.; Guilak, F. Site-Specific Molecular Diffusion in Articular Cartilage Measured Using Fluorescence Recovery after Photobleaching. *Ann. Biomed. Eng.* **2003**, *31* (7), 753–760. <https://doi.org/10.1114/1.1581879>.
- (47) Roughley, P. J.; Mort, J. S. The Role of Aggrecan in Normal and Osteoarthritic Cartilage. *J. Exp. Orthop.* **2014**, *1* (1), 1–11. <https://doi.org/10.1186/s40634-014-0008-7>.
- (48) Bajpayee, A. G.; Wong, C. R.; Bawendi, M. G.; Frank, E. H.; Grodzinsky, A. J. Avidin as a Model for Charge Driven Transport into Cartilage and Drug Delivery for Treating Early Stage Post-Traumatic Osteoarthritis. *Biomaterials* **2014**, *35* (1), 538–549. <https://doi.org/10.1016/j.biomaterials.2013.09.091>.

- (49) Vedadghavami, A.; Wagner, E. K.; Mehta, S.; He, T.; Zhang, C.; Bajpayee, A. G. *Cartilage Penetrating Cationic Peptide Carriers for Applications in Drug Delivery to Avascular Negatively Charged Tissues*; 2019; Vol. 93. <https://doi.org/10.1016/j.actbio.2018.12.004>.
- (50) Bajpayee, A. G.; Grodzinsky, A. J. Cartilage-Targeting Drug Delivery: Can Electrostatic Interactions Help? *Nat. Rev. Rheumatol.* **2017**, *13* (3), 183–193. <https://doi.org/10.1038/nrrheum.2016.210>.
- (51) Vedadghavami, A.; Mehta, S.; Bajpayee, A. G. Characterization of Intra-Cartilage Transport Properties of Cationic Peptide Carriers. *J. Vis. Exp.* **2020**, No. 162. <https://doi.org/10.3791/61340>.
- (52) Warren, M. R.; Vedadghavami, A.; Bhagavatula, S.; Bajpayee, A. G. Effects of Polycationic Drug Carriers on the Electromechanical and Swelling Properties of Cartilage. *Biophys. J.* **2022**, *121* (18), 3542–3561. <https://doi.org/10.1016/j.bpj.2022.06.024>.
- (53) Warren, M. R.; Bajpayee, A. G. Modeling Electrostatic Charge Shielding Induced by Cationic Drug Carriers in Articular Cartilage Using Donnan Osmotic Theory. *Bioelectricity* **2022**, *4* (4), 248–258. <https://doi.org/10.1089/bioe.2021.0026>.
- (54) Coughlin, J. E.; Reisch, A.; Markarian, M. Z.; Schlenoff, J. B. Sulfonation of Polystyrene: Toward the “Ideal” Polyelectrolyte. *J. Polym. Sci. Part A Polym. Chem.* **2013**, *51* (11), 2416–2424. <https://doi.org/10.1002/pola.26627>.
- (55) Kessler, C.; Ng, J.; Valdez, K.; Xie, H.; Geiger, B. The Use of Sodium Polystyrene Sulfonate in the Inpatient Management of Hyperkalemia. *J. Hosp. Med.* **2011**, *6* (3), 136–140. <https://doi.org/10.1002/jhm.834>.
- (56) Zairov, R. R.; Nagimov, R. N.; Sudakova, S. N.; Lapaev, D. V.; Syakaev, V. V.;

- Gimazetdinova, G. S.; Voloshina, A. D.; Shykula, M.; Nizameev, I. R.; Samigullina, A. I.; Gubaidullin, A. T.; Podyachev, S. N.; Mustafina, A. R. Polystyrenesulfonate-Coated Nanoparticles with Low Cytotoxicity for Determination of Copper(II) via the Luminescence of Tb(III) Complexes with New Calix[4]Arene Derivatives. *Microchim. Acta* **2018**, *185* (8), 386. <https://doi.org/10.1007/s00604-018-2923-2>.
- (57) Chouirfa, H.; Evans, M. D. M.; Castner, D. G.; Bean, P.; Mercier, D.; Galtayries, A.; Falentin-Daudré, C.; Migonney, V. Grafting of Architecture Controlled Poly(Styrene Sodium Sulfonate) onto Titanium Surfaces Using Bio-Adhesive Molecules: Surface Characterization and Biological Properties. *Biointerphases* **2017**, *12* (2). <https://doi.org/10.1116/1.4985608>.
- (58) Herold, B. C.; Bourne, N.; Marcellino, D.; Kirkpatrick, R.; Strauss, D. M.; Zaneveld, L. J. D.; Waller, D. P.; Anderson, R. A.; Chany, C. J.; Barham, B. J.; Stanberry, L. R.; Cooper, M. D. Poly(Sodium 4-Styrene Sulfonate): An Effective Candidate Topical Antimicrobial for the Prevention of Sexually Transmitted Diseases. *J. Infect. Dis.* **2000**, *181* (2), 770–773. <https://doi.org/10.1086/315228>.
- (59) Truong, N. P.; Jones, G. R.; Bradford, K. G. E.; Konkolewicz, D.; Anastasaki, A. A Comparison of RAFT and ATRP Methods for Controlled Radical Polymerization. *Nat. Rev. Chem.* **2021**, *5* (12), 859–869. <https://doi.org/10.1038/s41570-021-00328-8>.
- (60) Lo, C. Y.; Wu, Y.; Awuyah, E.; Meli, D.; Nguyen, D. M.; Wu, R.; Xu, B.; Strzalka, J.; Rivnay, J.; Martin, D. C.; Kayser, L. V. Influence of the Molecular Weight and Size Distribution of PSS on Mixed Ionic-Electronic Transport in PEDOT:PSS. *Polym. Chem.* **2022**, *13* (19). <https://doi.org/10.1039/d2py00271j>.
- (61) Jesson, C. P.; Pearce, C. M.; Simon, H.; Werner, A.; Cunningham, V. J.; Lovett, J. R.;

- Smallridge, M. J.; Warren, N. J.; Armes, S. P. H<sub>2</sub>O<sub>2</sub> Enables Convenient Removal of RAFT End-Groups from Block Copolymer Nano-Objects Prepared via Polymerization-Induced Self-Assembly in Water. *Macromolecules* **2017**, *50* (1), 182–191. <https://doi.org/10.1021/acs.macromol.6b01963>.
- (62) Poole, A. R.; Pidoux, I.; Reiner, A.; Tang, L. H.; Choi, H.; Rosenberg, L. Localization of Proteoglycan Monomer and Link Protein in the Matrix of Bovine Articular Cartilage: An Immunohistochemical Study. *J. Histochem. Cytochem.* **1980**, *28* (7), 621–635. <https://doi.org/10.1177/28.7.6156200>.
- (63) Volpi, N. Disaccharide Mapping of Chondroitin Sulfate of Different Origins by High-Performance Capillary Electrophoresis and High-Performance Liquid Chromatography. *Carbohydr. Polym.* **2004**, *55* (3), 273–281. <https://doi.org/10.1016/j.carbpol.2003.09.010>.
- (64) Maccari, F.; Volpi, N. Direct and Specific Recognition of Glycosaminoglycans by Antibodies after Their Separation by Agarose Gel Electrophoresis and Blotting on Cetylpyridinium Chloride-treated Nitrocellulose Membranes. *Electrophoresis* **2003**, *24* (9), 1347–1352. <https://doi.org/10.1002/elps.200390173>.
- (65) Volpi, N. Hyaluronic Acid and Chondroitin Sulfate Unsaturated Disaccharides Analysis by High-Performance Liquid Chromatography and Fluorimetric Detection with Dansylhydrazine. *Anal. Biochem.* **2000**, *277* (1), 19–24. <https://doi.org/10.1006/abio.1999.4366>.
- (66) Volpi, N. Quality of Different Chondroitin Sulfate Preparations in Relation to Their Therapeutic Activity. *J. Pharm. Pharmacol.* **2009**, *61* (10), 1271–1280. <https://doi.org/10.1211/jpp/61.10.0002>.
- (67) McIlwraith, C. W.; Frisbie, D. D.; Kawcak, C. E.; Fuller, C. J.; Hurtig, M.; Cruz, A. The

- OARSI Histopathology Initiative – Recommendations for Histological Assessments of Osteoarthritis in the Horse. *Osteoarthr. Cartil.* **2010**, *18* (4), S93–S105. <https://doi.org/10.1016/j.joca.2010.05.031>.
- (68) Schmitz, N.; Laverty, S.; Kraus, V. B.; Aigner, T. Basic Methods in Histopathology of Joint Tissues. *Osteoarthr. Cartil.* **2010**, *18* (SUPPL. 3), S113–S116. <https://doi.org/10.1016/j.joca.2010.05.026>.
- (69) Simkin, P. A. Synovial Perfusion and Synovial Fluid Solutes. *Ann. Rheum. Dis.* **1995**, *54* (5), 424–428. <https://doi.org/10.1136/ard.54.5.424>.
- (70) Maroudas, A. Distribution and Diffusion of Solutes in Articular Cartilage. *Biophys. J.* **1970**, *10* (5), 365–379. [https://doi.org/10.1016/S0006-3495\(70\)86307-X](https://doi.org/10.1016/S0006-3495(70)86307-X).
- (71) Seabra, I. J.; Gil, M. H. Cotton Gauze Bandage: A Support for Protease Immobilization for Use in Biomedical Applications. *Rev. Bras. Ciências Farm.* **2007**, *43* (4), 535–542. <https://doi.org/10.1590/S1516-93322007000400006>.
- (72) Kupratis, M. E.; Rahman, A.; Burris, D. L.; Corbin, E. A.; Price, C. Enzymatic Digestion Does Not Compromise Sliding-Mediated Cartilage Lubrication. *Acta Biomater.* **2024**, *178*, 196–207. <https://doi.org/10.1016/j.actbio.2024.02.040>.
- (73) Moody, H. R.; Brown, C. P.; Bowden, J. C.; Crawford, R. W.; McElwain, D. L. S.; Oloyede, A. O. In Vitro Degradation of Articular Cartilage: Does Trypsin Treatment Produce Consistent Results? *J. Anat.* **2006**, *209* (2), 259–267. <https://doi.org/10.1111/j.1469-7580.2006.00605.x>.
- (74) Rosenberg, L. Chemical Basis for the Histological Use of Safranin O in the Study of Articular Cartilage. *JBJS* **1971**, *53* (1), 69–82.
- (75) Sundar, S.; Linardi, R.; Gaesser, A.; Guo, T.; Ortved, K.; Engiles, J.; Parreno, J.; Dhong,

- C. Optics-Free, In Situ Swelling Monitoring of Articular Cartilage with Graphene Strain Sensors. *ACS Biomater. Sci. Eng.* **2023**, *9* (2), 1011–1019. <https://doi.org/10.1021/acsbiomaterials.2c01456>.
- (76) Crank, J. *The Mathematics of Diffusion*. 2nd Edn. **1979**. <https://doi.org/10.1088/0031-9112/26/11/044>.
- (77) Phillips, E. R.; Haislup, B. D.; Bertha, N.; Lefchak, M.; Sincavage, J.; Prudnikova, K.; Shallop, B.; Mulcahey, M. K.; Marcolongo, M. S.; Bui, T.; Taylor, A. J.; Galindo, D. A.; Huneke, R. B.; Hou, J. S.; Mulcahey, M. K.; Marcolongo, M. S. Biomimetic Proteoglycans Diffuse throughout Articular Cartilage and Localize within the Pericellular Matrix. *J. Biomed. Mater. Res. - Part A* **2019**, *107* (9), 1977–1987. <https://doi.org/10.1002/jbm.a.36710>.
- (78) Torzilli, P. A. Effects of Temperature, Concentration and Articular Surface Removal on Transient Solute Diffusion in Articular Cartilage. *Med. Biol. Eng. Comput.* **1993**, *31* (S1), S93–S98. <https://doi.org/10.1007/BF02446656>.
- (79) Stankovich, S.; Piner, R. D.; Chen, X.; Wu, N.; Nguyen, S. T.; Ruoff, R. S. Stable Aqueous Dispersions of Graphitic Nanoplatelets via the Reduction of Exfoliated Graphite Oxide in the Presence of Poly(Sodium 4-Styrenesulfonate). *J. Mater. Chem.* **2006**, *16* (2), 155–158. <https://doi.org/10.1039/B512799H>.
- (80) Torzilli, P. A.; Allen, S. N. Effect of Articular Surface Compression on Cartilage Extracellular Matrix Deformation. *J. Biomech. Eng.* **2022**, *144* (9). <https://doi.org/10.1115/1.4054108>.
- (81) Setton, L. A.; Zhu, W.; Mow, V. C. The Biphasic Poroviscoelastic Behavior of Articular Cartilage: Role of the Surface Zone in Governing the Compressive Behavior. *J. Biomech.*

- 1993**, *26* (4–5), 581–592. [https://doi.org/10.1016/0021-9290\(93\)90019-B](https://doi.org/10.1016/0021-9290(93)90019-B).
- (82) Lyyra, T.; Arokoski, J. P. A.; Oksala, N.; Vihko, A.; Hyttinen, M.; Jurvelin, J. S.; Kiviranta, I. Experimental Validation of Arthroscopic Cartilage Stiffness Measurement Using Enzymatically Degraded Cartilage Samples. *Phys. Med. Biol.* **1999**, *44* (2), 525–535. <https://doi.org/10.1088/0031-9155/44/2/017>.
- (83) Griffin, D. J.; Vicari, J.; Buckley, M. R.; Silverberg, J. L.; Cohen, I.; Bonassar, L. J. Effects of Enzymatic Treatments on the Depth-Dependent Viscoelastic Shear Properties of Articular Cartilage. *J. Orthop. Res.* **2014**, *32* (12), 1652–1657. <https://doi.org/10.1002/jor.22713>.
- (84) Ahmed, A. M.; Burke, D. L. In-Vitro of Measurement of Static Pressure Distribution in Synovial Joints—Part I: Tibial Surface of the Knee. *J. Biomech. Eng.* **1983**, *105* (3), 216–225. <https://doi.org/10.1115/1.3138409>.
- (85) Park, S.; Hung, C. T.; Ateshian, G. A. Mechanical Response of Bovine Articular Cartilage under Dynamic Unconfined Compression Loading at Physiological Stress Levels. *Osteoarthr. Cartil.* **2004**, *12* (1), 65–73. <https://doi.org/10.1016/j.joca.2003.08.005>.
- (86) Ackermann, B.; Steinmeyer, J. Collagen Biosynthesis of Mechanically Loaded Articular Cartilage Explants. *Osteoarthr. Cartil.* **2005**, *13* (10), 906–914. <https://doi.org/10.1016/j.joca.2005.06.001>.
- (87) Kikhney, A. G.; Svergun, D. I. A Practical Guide to Small Angle X-Ray Scattering (SAXS) of Flexible and Intrinsically Disordered Proteins. *FEBS Lett.* **2015**, *589* (19), 2570–2577. <https://doi.org/10.1016/j.febslet.2015.08.027>.
- (88) Wei, Y.; Hore, M. J. A. Characterizing Polymer Structure with Small-Angle Neutron Scattering: A Tutorial. *J. Appl. Phys.* **2021**, *129* (17). <https://doi.org/10.1063/5.0045841>.

- (89) Upadhyaya, R.; Murthy, N. S.; Hoop, C. L.; Kosuri, S.; Nanda, V.; Kohn, J.; Baum, J.; Gormley, A. J. PET-RAFT and SAXS: High Throughput Tools To Study Compactness and Flexibility of Single-Chain Polymer Nanoparticles. *Macromolecules* **2019**, *52* (21), 8295–8304. <https://doi.org/10.1021/acs.macromol.9b01923>.
- (90) Thünemann, A. F.; Knappe, P.; Bienert, R.; Weidner, S. Online Coupling of Field-Flow Fractionation with SAXS and DLS for Polymer Analysis. *Anal. Methods* **2009**, *1* (3), 177. <https://doi.org/10.1039/b9ay00107g>.
- (91) Chandran, P. L.; Horkay, F. Aggrecan, an Unusual Polyelectrolyte: Review of Solution Behavior and Physiological Implications. *Acta Biomater.* **2012**, *8* (1), 3–12. <https://doi.org/10.1016/j.actbio.2011.08.011>.
- (92) TANAKA, K. Physicochemical Properties of Chondroitin Sulfate. *J. Biochem.* **1978**, *83* (3), 655–659. <https://doi.org/10.1093/oxfordjournals.jbchem.a131956>.
- (93) Neumann, M. The Adsorption of Basic Dyes by Poly(Styrene Sulphonate). *Dye. Pigment.* **1992**, *20* (4), 255–260. [https://doi.org/10.1016/0143-7208\(92\)87024-U](https://doi.org/10.1016/0143-7208(92)87024-U).

## 11. TABLE OF CONTENTS GRAPHIC

For Table of Contents Only.

Kinetics and retention of polystyrene sulfonate for proteoglycan replacement in cartilage

*Shalini Sundar*<sup>1</sup>, *Allison Koopman*<sup>2</sup>, *Thomas J. Manzoni*<sup>3</sup>, *Weiran Xie*<sup>2</sup>, *Qurat-Ul-Ain Bhatti*<sup>2</sup>,  
*Chun-Yuan Lo*<sup>4</sup>, *Vidhika S. Damani*<sup>2</sup>, *Ai Nin Yang*<sup>4</sup>, *Darrin Pochan*<sup>2</sup>, *Justin Parreno*<sup>1,3</sup>, *Julie B.*  
*Engiles*<sup>5,6</sup>, *Laure V. Kayser*<sup>2,4</sup>, *Charles Dhong*<sup>\*1,2</sup>

